Materials Physics and Mechanics. 2022;48(2): 242-271
Research article
http://dx.doi.org/10.18149/MPM.4822022_9

Received: October 9, 2021
Accepted: April 13, 2022

FAILURE ANALYSIS OF SEMI-ELLIPTICAL CRACK BEHAVIOR IN THE CEMENT MANTLE OF A TOTAL HIP PROSTHESIS

Samir Zahaf[1]✉, Mouloud Dahmane[2], Azzeddine Belaziz[3], Ismail Bouri[4], Nasreddine Afane[5]

[1]Department of Technology, University of Djilali Bounaama-KhamisMeliana, AinDefla-Algeria

[2]Department of planning and hydraulic engineering, Higher National School of Hydraulics, Blida 9000, Algeria; LMA, USTO-MB, Oran 31000, Algeria

[3]Mechanical Research Center Constantine (CRM), University campus of châaberssas, Constantine, 25017, Algeria

[4]Department of Mechanical Engineering, Mostaganem University-Abdelhamid Ibn Badis, Algeria

[5]Department of Mechanical Engineering, National Polytechnic School of Oran -MA, BP 1523 ElMnaour, Oran, Algeria

✉ samir.zahaf@univ-dbkm.dz

Abstract. Numerical modeling by finite element method offers valuable information and details on the mechanical behavior of the prosthesis in terms of stress and strain distribution, load transfer, stress intensity factors, etc. An explicit analysis conducted on the behavior of microcavity and cracking in PMMA surgical cement (polymethyl methacrylate) used for a total hip prosthesis (THP) is of great importance in collecting information about the nature of the loosening phenomenon of the cement application. The rupture of orthopedic cement is practically the main cause of this loosening. Understanding the different failure mechanisms provides a significant advance in the cemented total prostheses. To do this, a numerical analysis by 3D finite element method (FEM) model of the total hip prosthesis was carried out in order to evaluate the stress levels in the different components. We focused on the effect of the microcavity rotation and the semi-elliptical crack position on the stress distribution in THP elements and on the orthopedic cement, which represents the weakest link of the prosthesis. We concluded that the two mechanical defects (Microcavity, semi-elliptical crack) exhibit more intense stresses in the THP components and record a very intense stress level and stress intensity factor KI. These mechanical defects causing damage to the PMMA around the tip of the bone debris increase the loosening state of the total hip prosthesis.

Keywords: finite element method, mechanical, crack, microcavity, prosthesis, orthopedic cement, stress von Mises, strain, stress intensity factors

Acknowledgements*. No external funding was received for this study.*

Citation: Zahaf S, Dahmane M, Belaziz A, Bouri I, Afane N. Failure analysis of semi-elliptical crack behavior in the cement mantle of a total hip prosthesis. *Materials Physics and Mechanics.* 2022;48(2): 242-271. DOI: 10.18149/MPM.4822022_9.

Abbreviation:
(THP): total hip prosthesis, (FEM): finite element method, (SIF): stress intensity factors, (THR): Total hip replacement, (THA): total hip arthroplasty, (PMMA): polymethyl-methacrylate, PEEK: Polyether Ether Ketone, (TKA): total knee artificial, (UHMWPE): Ultra High Molecular Weight Polyethylene, coxal-bone (pelvis).

1. Introductıon

Total hip replacement is an intervention of a biological articulation with a prosthesis; her effectiveness depends on the quality of reconstruction, architecture, the mechanics of the hip, integrity, and equilibrium, for those used as medical implants for orthopaedic and dental surgery (80,000 hip replacements and 30,000 knee prostheses are implanted annually worldwide). According to the Swedish register of total hip replacement over a period of 19 years, 7.1% of patients who underwent cement less total hip arthroplasty will need a second surgery for replacing the first; this number is 13% for patients who underwent cement less (THA). The main reason for revisions (THA) is aseptic loosening in 71% of cases, followed by infection in 7.5% (Herberts and Malchau, 2000 [1]).

During a total hip arthroplasty, the surgeon replaces the two surfaces of the natural joint produced by the interlocking of the femoral head in the acetabulum of the hip iliac bone with two prosthetic components [1-5], Fig. 1:

- The cup is placed in the acetabulum after removal of the cartilage: this is the fixed part of the joint.
- The femoral implant is anchored in the medullary canal after resection (surgical removal) of the femoral neck and partial recess of the canal: this is the mobile part.

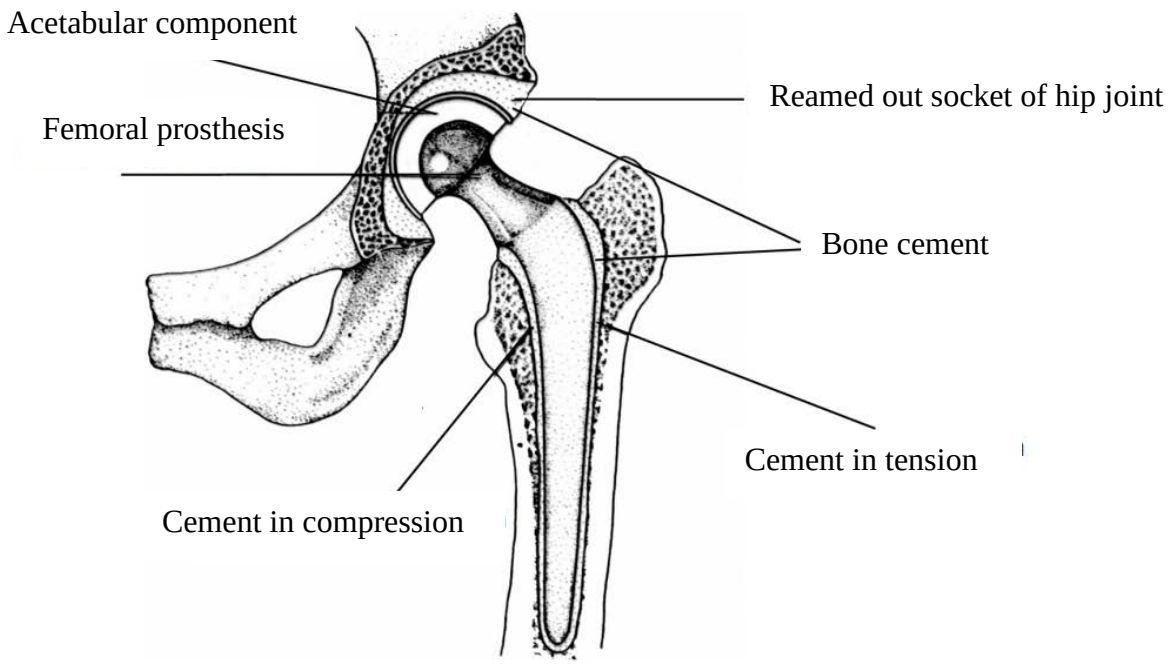

Fig. 1. Schematic diagram of prostheses and polymethyl-methacrylate (PMMA), bone cement in an acetabular socket and femur [6]

Operation of total hip replacement shows the increasing numbers and be successful. The cemented system is most widely used in total hip replacement. Reliability of the THR is important to the patient, orthopedics, and surgeons. Therefore, improved design, technology, and materials for inserting hip replacements are highly needed. This also includes whether the

design of the THR is cemented or uncemented. Bone cement is widely used to affix hip implants to the bone during total hip arthroplasty; therefore, many studies have been performed to investigate the reliability of cement mantle in a total hip replacement [7-8].

Sir John Charnley et al. used a cold-curing acrylic resin, surgical-grade polymethyl-methacrylate, for the fixation of prostheses in the supporting bone, that the long term stability of metal implants was achieved. PMMA is the only material currently used for anchoring prostheses in bone during cemented arthroplasties [9].

Fisher et al. observed the effect of the cement mantle thickness on strains on total hip replacement experimentally on stem components. The study was conducted on two stem components by varying the thickness of the cement mantle. Strain gauges were embedded in the cement mantle, and then the stem components were subjected to an axial load in walking and standing conditions.

The results showed that an increase in cement mantle thickness from 2.4 to 3.7 mm can decrease the strain on the cement mantle by about 40%-49%, so they concluded that by increasing cement mantle thickness the fatigue life of an implant may be increased [10].

Jamari et al. studied and analyzed an additional layer of cement mantle hip joints to reduce cracks [11]. A previous study showed that adding a metallic layer between the liner and the acetabulum could reduce the stress at the contact surface of the cement mantle. Several material properties of the layer were simulated using finite element analysis for maximum performance. Static contact analysis was used to simulate the stresses at the contact surface of the cement mantle. The results show that an additional layer of cobalt-chromium produced the best performance.

Ajay Kumar et al. studied and analyzed the effects of interfacial crack and implant material on mixed-mode stress intensity factor and prediction of interface failure of the cemented acetabular cup. A three-dimensional (3D) finite element (FE) model of implanted pelvic bone was developed based on the computed tomography (CT) scan data. Combinations of four materials were considered for implant material. The results show that the material properties of the implant play a vital role in interface failure. The values of KI and KII decrease as the implant material changes from UHMWPE-CoCrMo to the ceramic–ceramic material combination. This result suggested that the ceramic–ceramic material combination will perform better than other combinations [12].

Abdel-Wahab and Silberschmidt experimentally and numerically studied the dynamic behavior of a fracturing impact in the cortical bone tissue, using X-FEM [13]. Another study by Milena Babić et al. studied the fatigue life of a loosened total hip prosthesis femoral component cemented into bone and was investigated assuming loads specified by the standard ISO 7206-4. The total hip prosthesis CAD model was developed by implementing a 3D scanning procedure. Based on the created CAD model, the FE model was developed. A linear elastic analysis was carried out for the created FE model of the prosthesis. The analysis showed that high tensile stresses occur on the distal region of the femoral component shaft on the anterior lateral side, where fatigue cracks occur in real cases. This procedure can be implemented in other components where the geometry needs to be reconstructed by 3D scanning [14].

Ramos et al. experimentally observed that the position of an implant in the femur and assemblage with the femoral canal were two important issues in the formation mechanism of cracks between the two surfaces (bone-cement, cement-implant) [15].

Griza et al. analysed with FEM the stress distribution of the acetabular part in the (THP) using screw fixation. The analysis showed that it took a large amount of computational force to predict screw fracture in the case of the unbounded metal-backed and bone interface [16].

Latham Krista et al. Modelling of femur fracture using finite element procedures [17].

Najafi et al. simulated the cortical bone with the presence of micro-cracks. They showed that cracks propagation was strongly influenced by bone density, thus, suggesting that bone fracture toughness should be provided, at least in part, in such a manner that bone density could be quantified [18].

Milena Babić et al. studied and analyzed a fracture by the finite element of a loosened femoral component shaft of the total hip prosthesis damaged with a crack was performed assuming loading and boundary conditions given by the standard ISO 7206-4. In the femoral component shaft, a damaged crack was modelled, where several crack depths were considered. Mode I stress intensity factor KI values were calculated for nodes along the crack front for each of the considered crack depths. It was demonstrated that for the given loading conditions a critical crack size associated with fracture onset could be estimated [19]. Several experimental procedures have been carried out on the cement, showing the existence of cracks emanating from cavities within the body (McCormack and Prendergast, 1999). These cracks are mainly responsible for the loosening of the total hip prostheses [20].

EkoSaputra et al. investigated the effect of the layer variation between the liner and the cement mantle on the reduction of hip joint cracks in polymethyl-methacrylate material. Failure of cement mantle, and bond loosening between liner and cement mantle are important issues in total hip replacement. Two factors that are common because of cement mantle failure are initial crack and stress. A solution for reducing stress on the cement mantle consists to insert the material between the liner and cement mantle. Nevertheless, further study is needed to optimize the proposed solution. A potential option is to vary the insertion material thickness. If the polymethyl-methacrylate material thickness is constant, the insert thickness variation will be followed by the liner thickness variation. Consequently, the stress value in the liner will follow the liner thickness variation. Results revealed that stress magnitude and deflection decreased in the cement mantle and the liner with insert material thickness increased [21].

Lennert de Ruiter et al. studied and determined the quality of the implant-cement interface of a PEEK femoral TKA component and compare it to a CoCr implant. Implants were subjected to clinically relevant loading and motions for up to 10 million cycles (MC) in a knee simulator and a method was developed to assess the bonding between the implant and cement and the integrity of the cement mantle. It was hypothesized that, due to the difference in thermal conductivity and modulus of the implant materials, the bonding at the cement-implant interface and the cracking of the cement would differ between implant materials and that PEEK would show more debonding and cracks in the cement mantle than CoCr. This was a preliminary study to establish a method to evaluate the implant-cement interface and as such was carried out with small sample size. The results show poor initial bonding of the PEEK-cement interface; however, after 10 MC simulations, the bonding of the implant remained similar to that of the controls. For CoCr implants, good fixation was measured for the gait control samples, but, after 10 MC, substantial implant–cement interface debonding occurred. After 10 MC, there was no significant difference in implant–cement debonding for the femoral component materials investigated, nor were there significant differences in macroscopic damage of the cement mantle. Further investigations either using a more physiologically relevant simulation system or through either animal studies or a clinical trial may be necessary to confirm these findings [22].

Aleksandar Sedmak et al. studied and analysed fatigue crack growth in hip implants by the extended finite element method. Toward, the three-dimensional finite element model is created and used in ABAQUS and Morfeo/crack add-in for ABAQUS to simulate fatigue crack growth from initial value up to the critical point. Initial crack dimensions are assumed according to the experience with failures of hip implants, whereas the final, critical value was estimated using data for fracture toughness obtained by experimental testing of hip implants

made of Ti-6Al-4V alloy. Results for the equivalent stress intensity factor and number of cycles in each of 40 steps of fatigue crack growth are presented and analysed, indicating the point of unstable crack growth [23].

SaitKocak et al. investigated the strength effect of both implant-cement and cement-bone interfaces in a cemented implant. The effects of different implant materials, blasting sand particle size and cement mantle thickness on strength impact were investigated. The results show that surface roughness values of implant materials increased as larger blasting sand particles were applied. On the other hand, interfacial strength impact increase with surface roughness increase. The cement-bone interface strength was higher than the implant-cement interface. The optimum mantle thickness in terms of impact strength was found to be 2 mm under impact force, failure will occur at the implant-bone cement interface [24].

Cherfi et al. studied the effect of inclusion in some cement zones where loading conditions can lead to crack opening leading to their propagation and consequently aseptic THR loosening. The fracture behavior of bone cement includes a strange body (bone remains) from which crack onset is supposed. The loading conditions effect, geometry, presence of both crack and inclusion on stress distribution, and fracture behavior of the cement. The results obtained by the authors indicated that the highest stresses are located around the sharp tip of bony inclusion. Most critical cracks are located in the middle of the cement mantle when they are subjected to one leg standing state loading during walking [25].

Ali Benouis et al. studied the cracks behavior, initiated in the cement connecting the femoral stem with the bone, using FEM analysis. Their study is focused on stress intensity factor variation in modes I, II, and III. This rupture criterion is used according to crack nature, orientation, and location in the orthopedic cement. First, the von Mises stress level and distribution are analyzed, induced in the medial, proximal, and distal parts of the bone cement. Then, the behavior of different geometric forms of an elliptical crack is evaluated which are located and initiated within the body of these three parts [26].

Among the problems encountered by experts in cemented arthroplasty is the occurrence of defects in the cement. These defects can locally generate stress concentration zones producing potential cement rupture. In general, there are three defect types: porosities, inclusions, and cracks [26]. It is well known that cracks are the most dangerous defects due to high induced stress intensity. Three types of cracks can be identified in orthopedic cement [27]:

- Cracks initiated on voids (cavities during shrinkage).
- Cracks initiated during cement polymerization, when it has not yet hardened.
- Cracks initiated in the cement due to internal stresses.

Crack propagation can lead to abrupt rupture, and then prosthesis loosening. The concept of linear elastic fracture mechanics, such as stress intensity factors, the rate of energy release, etc., accurately describes crack behavior in brittle materials according to geometry and loading conditions.

The use of these concepts can be an effective tool to analyze orthopedic cement fracture behavior, which provides a predictive tool for an effective assessment of pre/post-cemented acetabular reconstruction operations. Despite numerous studies on cement fatigue [28] and developed finite element models of damage increase in the cement mantle [29], crack propagation has not yet been addressed using appropriate fracture mechanics techniques [30].

1-The aim of this study is to carry out a numerical study on the effect of femoral stem position on stress distribution in the orthopedic cement without defects. Next, we will present a detailed analysis of the microcavity position effect in the cement in order to locate stress concentration areas that represent potential sites of damage and microcracks initiation.

2- Crack behavior analysis in the reconstructed acetabular cement by stress intensity factor and J-integral assessment along the crack front. The finite element method is used to achieve this goal. The effects of both crack positions have been highlighted.

2. Three-dimensional numerical model

Geometrical model and boundary conditions. The three-dimensional geometrical model of the hip prosthesis is shown in Fig. 2 and Fig. 3. A polyethylene cup with an outside diameter of 54 mm had been sealed to an acetabulum of diameter 56 mm. The normal weight of a man with this acetabulum diameter is around 80 kg [29]. The cement layer thickness is 3 mm while the cup's internal diameter is 28 mm [30].

Figure 2 (a) and (b) show the reconstructed acetabulum geometrical model. This model has the advantage of getting closer to the real structure. The total hip prosthesis components are hip bone, cement, implant, and cup are clearly defined. The reliability of obtained results requires a very refined mesh, especially at the cement level considered as a determining prosthesis element.

The boundary conditions used in our case are:

1. A fixed embedment (Ux = Uy = Uz = Rx = Ry = Rz = 0) on the pubis and on the iliac bone wing (see Fig. 4 (b)).
2. A concentrated load of 2400N was applied to the implant (see Fig. 4 (b)) [31].
3. We considered continuous rigid contact at the bone-cement and cup cement interfaces and a frictionless and non-interpenetrable interaction at the implant-cup interface (these conditions made by the code Ansys Workbench).

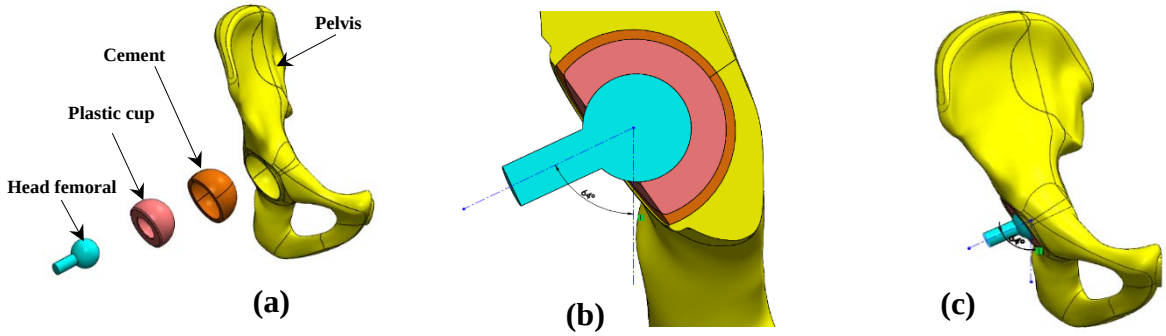

Fig. 2. 3D model of the total hip prosthesis by software SolidWorks, (a): exploded view of the THP, (b): cross-sectional view, (d): assembled view

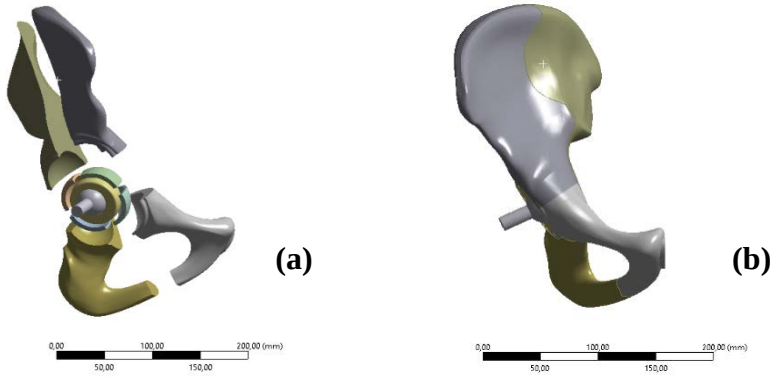

Fig. 3. Geometric model of the total hip prosthesis by the code AnsysWorkbench, (a): exploded view, (b): isometric view

This model permits the reproduction of all movement phases by just changing the applied force direction [32]. The loading cases analyzed in this study correspond to $\alpha = 64°$ (femoral head is in contact with one end of the cup). A large area of the cement's left part is under tension. It is generally known that cement does not well withstand tensile loading. The cement tensile, compressive, and shear strength are 25 MPa, 80 MPa, and 40 MPa respectively [33].

Finite Element Model. Numerical methods such as the finite element method are widely accepted in orthopedic biomechanics as an important tool used to design and analyze prosthesis mechanical behavior [34]. Several authors have used this method to analyze hip prosthesis mechanical behavior, Colombi [35-40].

The contribution in this area is based on crack behavior analysis in the cement layer which connects the acetabular cup to the adjacent bone, by evaluating the stress intensity factor along the crack front. This was done using the commercial finite element AnsysWorkbench [41-46]. A three-dimensional finite element model of the reconstructed acetabulum is studied, Fig. 4 (a). A 10-node tetrahedral element is used to mesh the hip bone and all other prosthesis components (Fig. 4 (a)). An appropriate refined mesh is performed in the cement, cup, and femoral stem to improve accurate results, Fig. 4 (a).

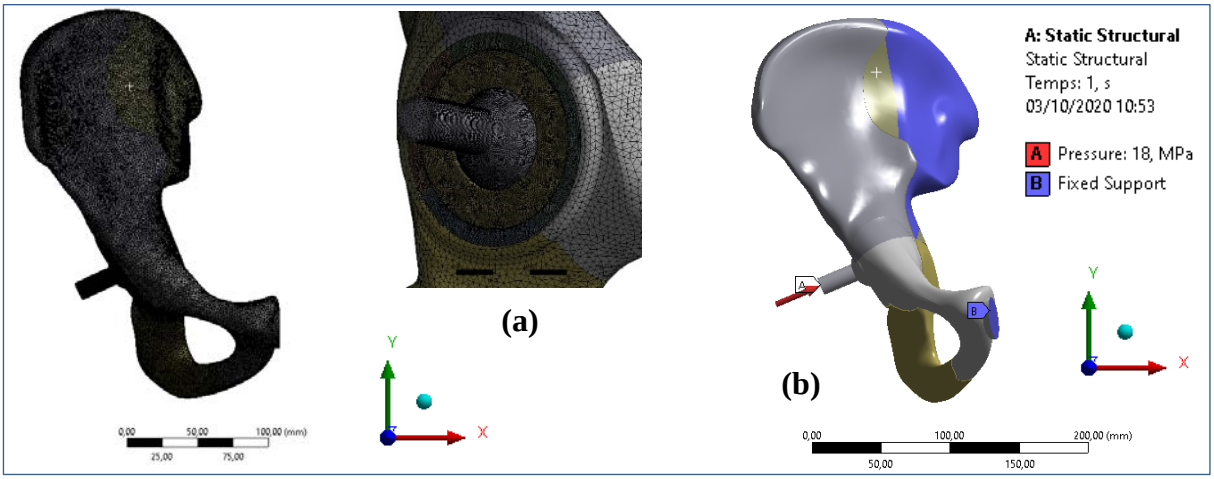

Fig. 4. (a): Total hip prosthesis mesh, (b): boundary conditions

3. Material Properties

Several types of materials were used for prosthesis components in this simulation. These materials are summarized in Table 1. All previous studies have assumed that the coxal-bone (pelvis) is divided into two components (cortical and cancellous) and each component takes on an elastic and isotropic behavior. Consequently, knowledge of the stress intensities and their distribution in the cement fixing the cup is of great importance for understanding the condition of the prosthesis in service and its loosening. On the other hand, for the boundary conditions, i.e. a fixed embedding at the level of the pelvis plus a force F is applied to the center of the femoral head, the interfaces between the cement, the pelvic bone, the plastic cup are perfectly glued (completely bonded). However, in this study, we propose that the coxal bone contains a single solid element called the cortical bone, which takes on an elastic and isotropic behavior. According to Anderson et al. [47], Fadela Allaoua et al. [48], and Ouinas et al. [49], the coxal bone has an elasticity modulus of 20000 MPa and Poisson's ratio of 0.25. Material for the cement mantle is adopted from Fadela Allaoua et al. [48], Ouinas et al. [49], and Azari Fahimeh et al. [50] with Young's modulus ranging from 2000 to 2300 MPa and Poisson's ratio of 0.3. Cement properties are: tensile strength 25 MPa, compressive strength 80 MPa (Rodriquez et al. [51]), shear strength 40 MPa (Merckx, [52]) and fatigue

(108 cycles) 14 MPa (Pilliar et al. [53], Solt´esz. [54]). Ries et al. [55] found that the critical stress intensity factors KIC are between 0.96 MPa√m to 1.76 MPa√m. The plastic cup has an elasticity modulus of 750 MPa and Poisson's ratio of 0.25. The cement, plastic cup, and femoral head are considered linear isotropic elastic materials.

Table 1. Elastic properties of materials

Materials	Young's modulus E [MPa]	Poisson coefficient *v*
Plastic cup	750	0.25
Cement (PMMA)	2000	0.25
coxal bone	20000	0.25
femoral head	210000	0.3

Effect of implant position. The analysis of the stress distribution in the different cavities of the orthopedic cement of the acetabular part requires different types of loading, characterized by the position of the neck of the implant with respect to the cup axis (Fig. 5). We have opted for three defined orientations of 0°, 10°, 20°, 30°, and 40° respectively which reflect human body postures.

The distribution and the level of stress in the orthopedic cement of the THP, according to these orientations were carried out by the finite element method.

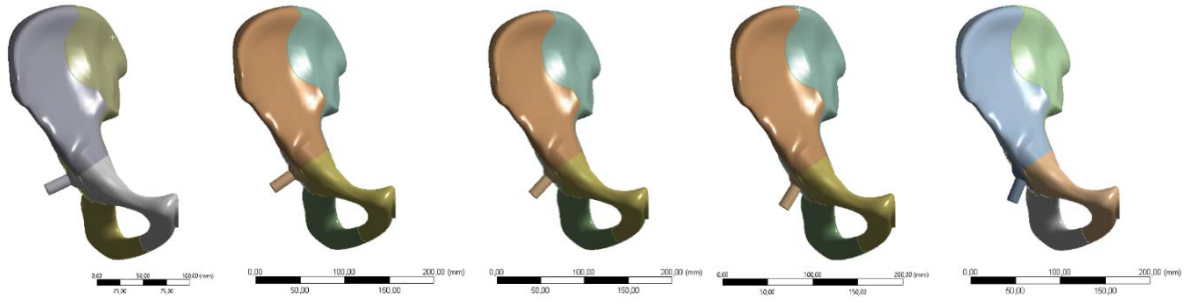

(a) **(b)** **(c)** **(d)** **(e)**

Fig. 5. Implant position with respect to the cup axis (a): α = 0°, (b): α = 10° (c): α = 20° and (d): α = 30°, (e): α = 40°

4. Results and Discussions

Distribution of von Mises stress in the hip bone-prosthesis structure. We analyzed distribution and stress level for the first implant position (alignment of the implant neck on the cup axis, characterized by an orientation angle α = 0°) Fig. 5 (a).

The latter shows that von Mises equivalent stress distribution is not homogeneous throughout the coxal bone-THP junction. High stresses of 44.453 MPa value are located in the femoral stem (outline in red). This results from the application of the concentrated load on a small area of the femoral neck. This stress will be transmitted from the implant neck to other prosthesis components. In the pelvis, maximal stresses are in the pelvis bone (approximately 19.48 MPa) see Fig. 7(a).

The second implant position corresponds to a neck implant orientation of 10° with respect to the cup axis. Results showed the equivalent stress distribution in the entire coxal bone junction. THP reaches a von Mises stress of 44.06 MPa due to the contribution of THP system components. The third position of the implant corresponds to a 20° orientation of the implant neck relative to the axis of the cup. Such an orientation favors the increased stresses by the embedding Fig. 6 (c). We find that compared to an alignment of the implant on the axis

of the cup, the stress intensity can reach too high a level (around 121.12 MPa) greatly exceeding the actual values.

This results from the application of the concentrated load on a small area of the femoral neck. This stress will be transmitted from the neck of the implant to the other components of the prosthesis. At the level of the right hip bone, the greatest stresses are located in the hip joint (approximately 36.64 MPa). The four-position of the implant is characterized by a strong orientation (30°) of the implant relative to the cup. Under this effect, the implant abuts the upper part of the cup (Fig. 6 (d)). This area is highly stressed; such behavior leads to a degradation of the equivalent stress.

The greatest stress, on the order of (48.55 MPa), is exerted on the complete structure of the coxal bone-THP. The remaining part of the structure is subjected to relatively low equivalent stress (less than 18.187 MPa).

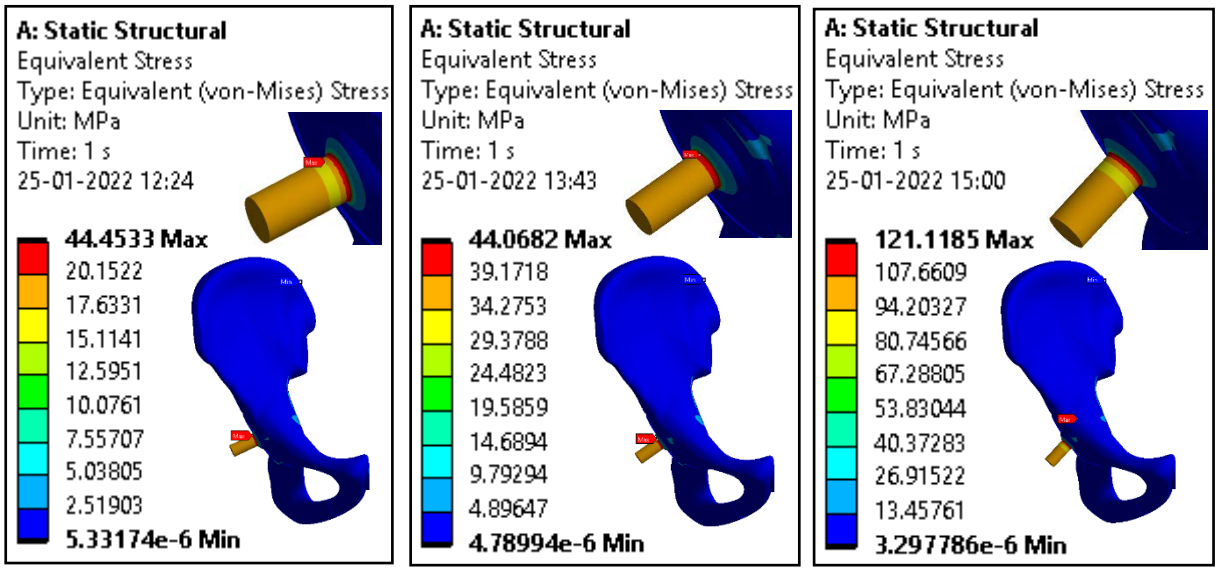

(a) : Position α =0° **(b) : Position α =10°** **(c) : Position α =20°**

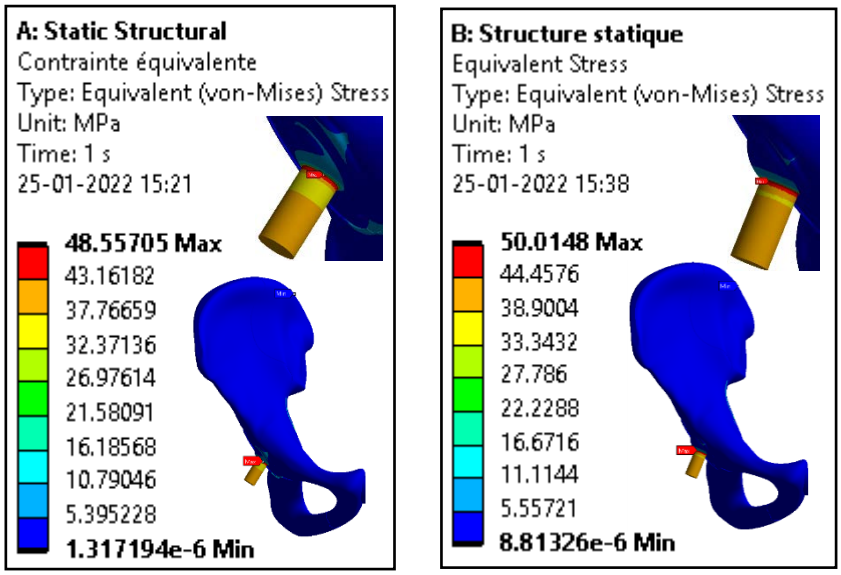

(d) : Position α =30° **(e) : Position α =40°**

Fig. 6. Implant orientation effect on equivalent stress distribution in hip bone-prosthesis structure

The fifth position of the implant corresponds to an orientation of 40° of the neck of the implant with respect to the axis of the cup showing that the distribution of the von Mises equivalent stress throughout the coxal bone-THP junction is 50.01 MPa by the contribution of the other components of the THP system. This stress will be transmitted from the neck of the implant to the other components of the prosthesis. At the level of the pelvis, the strongest stresses are located in the coxal bone (approximately 12.44 MPa) see Fig. 7 (e).

Distribution of von Mises stresses in the coxal bone (pelvis).

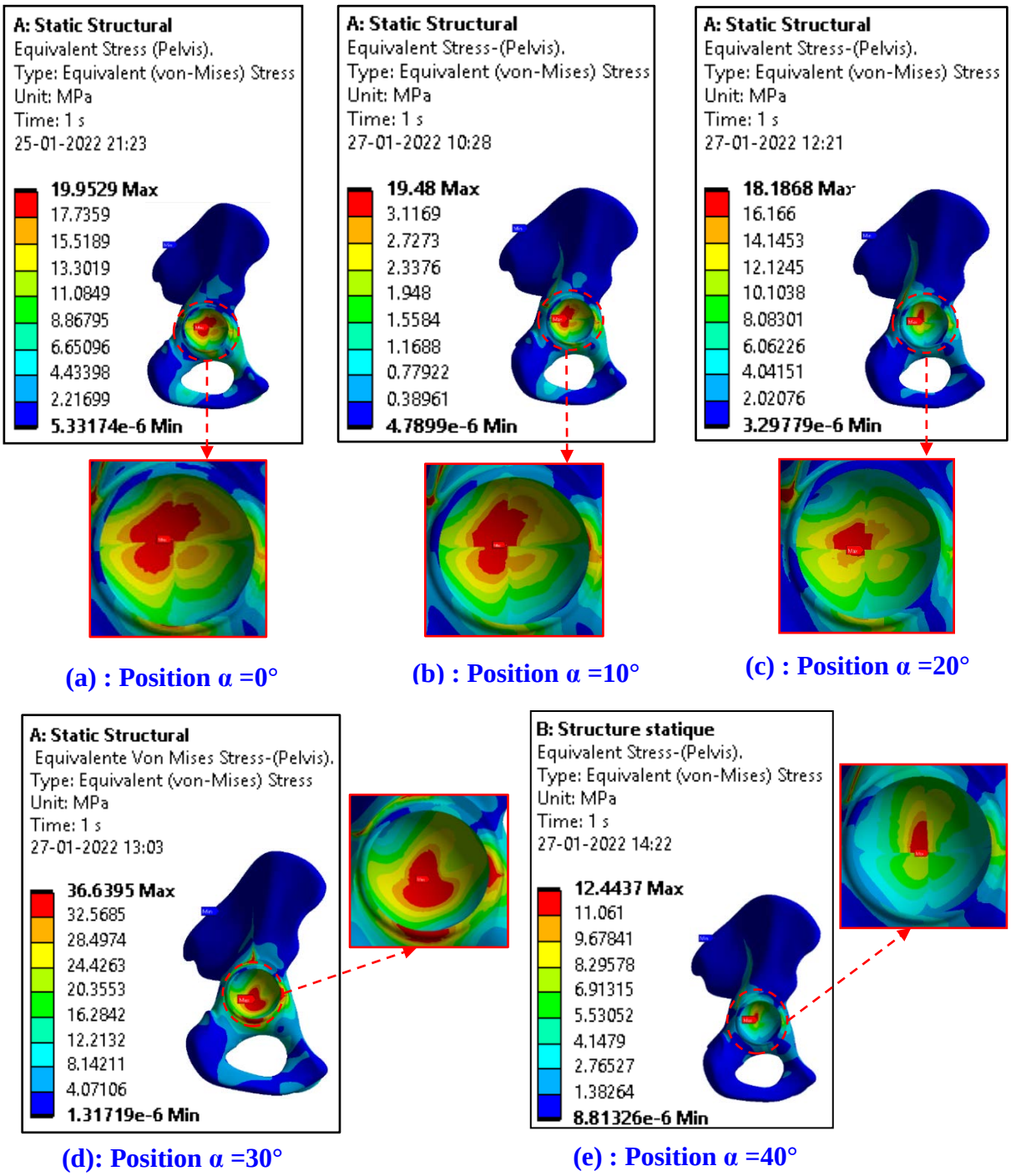

Fig. 7. Effect of implant orientation on the distribution of equivalent stress in the coxal bone (pelvis)

Distribution of stress von Mises in cement (PMMA). Cement is a very determining element of THP. Its analysis is of great importance for the life of the prosthesis. Therefore, we have studied the distribution and intensity of stresses in cement (Fig. 8). In the case of alignment of the implant on the axis of the cup, an area of the cement is under high stress; is in the direction of the load application. It is in this region that the stresses are greatest and are intensively localized at the cement-bone interface. In the rest of this structure, the stresses remain very low (Fig. 8 (a)). In 0° position, the stress is equal to 4.69 MPa.

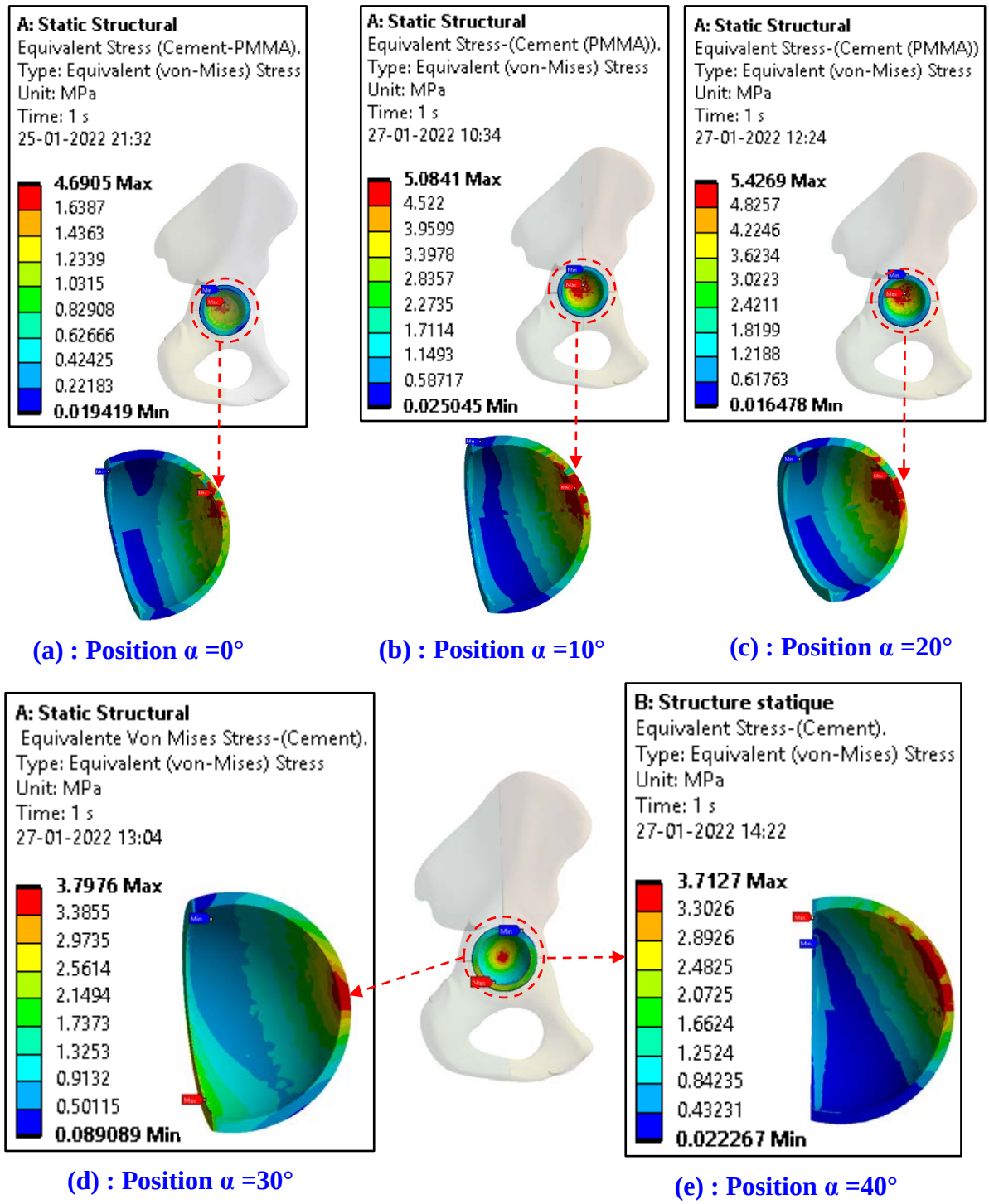

Fig. 8. Effect of implant orientation on the distribution of equivalent stress in the cement

An increase in the orientations of this implant (10°, 20°) generates the most significant stress, located in the region subjected to mechanical loading with a greater amplitude than that resulting from the first stress and its effect is less extensive. The upper part of cement is the site of stress concentration, due to both the compressive stress field between the cup and the implant. It is in this part of the cement and near the interface with the coxal bone that the equivalent stress is strongly localized (Fig. 8 (b,c)). In this case, the stresses of von Mises are equal to (5.08MPa, 5.42MPa).

The equivalent stress is intensively localized in the convex part of the cement located in the direction of this inclination and more particularly at the cement-cup interface in its close vicinity (Fig. 8). At this level, a significant reduction in the von Mises stress compared to the first and second loading was noticed. This can be justified by the fact that the implant is almost along the axis consisting of the pubis and the iliac wing, eliminating the damping effect seen in the first case. The maximum stress is 3.79MPa, and 3.71MPa.

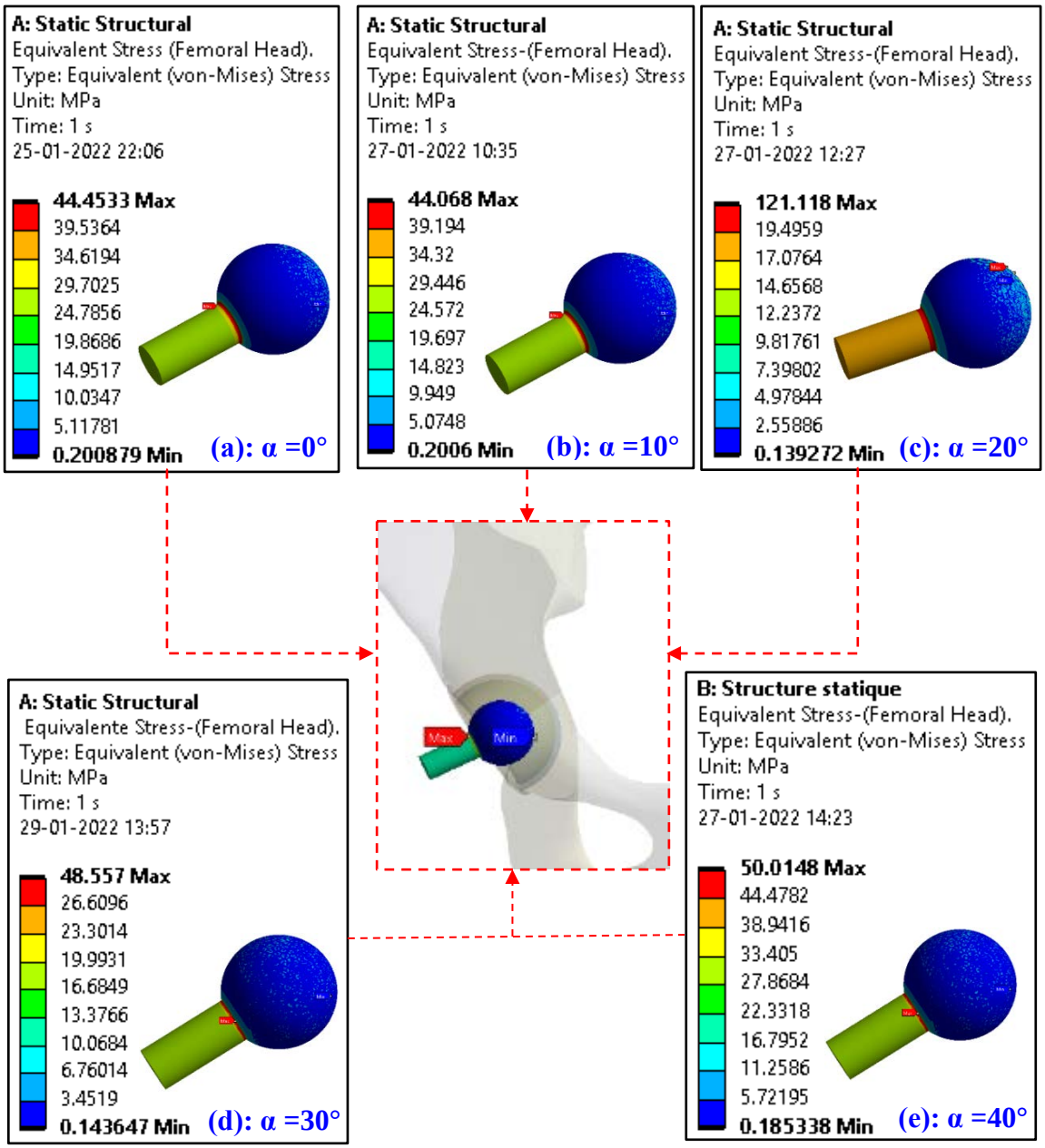

Fig. 9. Effect of implant orientation on the distribution of equivalent stress in the femoral stem

Distribution of stress von Mises in femoral stem. The results obtained for the analysis of the von Mises equivalent stress distribution in the implant are shown in Fig. 9. We find that the implant-cup axis alignment of (0°, 10°) results in a very small variation of the equivalent stress in the neck of the implant and in its extension in the femoral head (Fig. 9 (a,b)).

The stress is weakly concentrated on the sharp edges between the neck and the head of the implant. Orientation of the implant at 20° results in a very strong variation of the equivalent stress in the neck of the implant and in its extension in the femoral head which is equal to 121.12 MPa (Fig. 9 (c)).

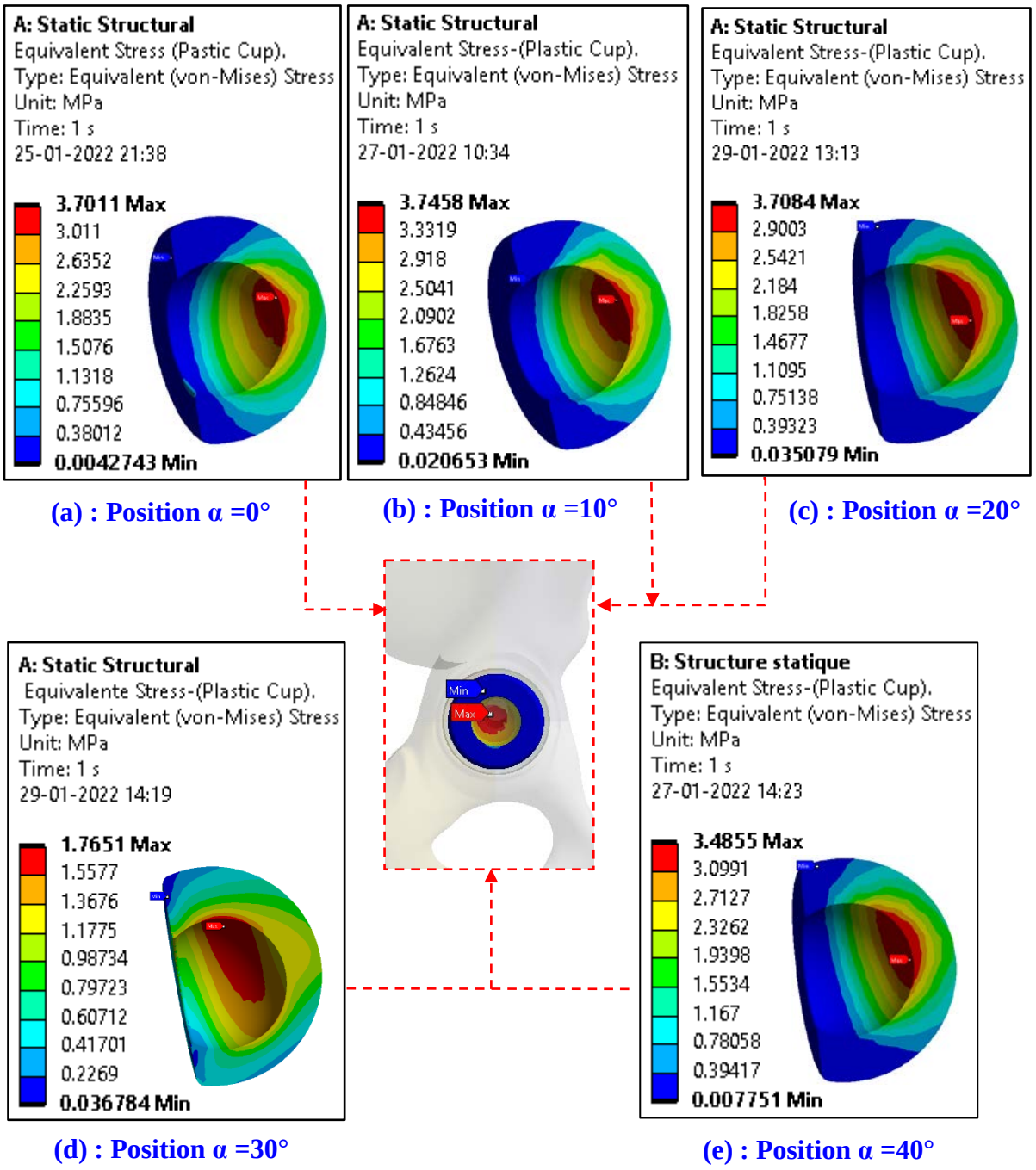

Fig. 10. Distribution of the equivalent stress in the plastic cup

For the two orientations 30° and 40°, the von Mises stresses are stable and concentrated on the sharp edges between the neck and the head of the implant (see Fig. 9 (d,e)). Orientation of the implant at 30° and 40° (Fig. 5 (d,e)) does not cause any variation in this constraint regardless of the degree of inclination. This behavior is explained by the fact that the loading in this area has not changed.

Distribution of the equivalent stress in the plastic cup. In this section, an analysis of the stress distribution in the cup made of very high molecular weight polyethylene (UHMWPE: Ultra High Molecular Weight Polyethylene) as a function of the position of the implant with respect to the axis of the cup has been carried out. The results of this analysis show that the equivalent stress is more significant are located near the contact area with the femoral head (Fig. 10).

This behavior is due to the effects of the compressive stresses generated by the head of the implant on one side, and tensile stresses resulting from the fixation of the pubis on the other hand. Noting that the intensity of this stress remains low and does not constitute any danger for the patient.

The influence of the orientation of the implant on the distribution and the equivalent stress intensity in the cup was illustrated in Fig. 10. Compared to the first and the second mechanical solicitation (Fig. 10 (a)) and (Fig. 10 (b)), the third loading (Fig. 10 (c)) generates intensity and distribution stress constant (3.74MPa, 3.7MPa, 3.7MPa). However, the contact area with the implant head is subjected to compressive stresses. The high values recorded in this part are due to the contact effect.

The traction of the cup with the bone in the lower area of the cup is responsible for the increase in equivalent stress. In its upper part, the cup is more stressed. A strong orientation of the implant (Fig. 10 (d)) results in the intensification of the stresses which are located almost on the upper surface of the cup near the cup-head interface of the implant. It is of less intensity compared to those induced by the first and second orientation. The position of high-stress concentration is located in the area of application of the contact force of the cup with the head of the implant.

Effect of micro-cavities.

Effect of cavity location on stress distribution. Polymethyl-methacrylate (PMMA) is the only material currently used for fixing prostheses in bone during cementing arthroplasty; this connection is carried out via a mechanical coupling of cement overlay to bone surface defects (anchor). Roughness is a determining parameter for fastening the bone-cement-implant system; it can lead to a more secure cement attachment [56], but can also be a source of crack initiation due to the notch effect in cement, which can lead to loosening [57].

Cement is the weakest link of the chain transfer load implant-bone-cement, its damage is responsible for loosening the interface at the cement-implant where micro-cracks over time fatigue develop greater extent and take more significant sizes. These cracks lead to both cement destruction and implant mobility within the bone. Such behaviour results in a pelvic fracture in the patient [58] with intolerable pain.

Several types of research were dedicated to the analysis of cement damage, which is largely responsible for total hip prosthesis loosening.

Other numerical work [59-60] showed that the existence of microcavity promotes the initiation and propagation of cracks in the cup of cement. The stress intensity factor is strongly influenced by the nature of the bone-cement interface, cement-implant. Propagation mode is dependent on the priming site of the cracks initiated micro-cavities.

The study and analysis of the intensity and distribution of von Mises stresses are made according to the position of the microcavity in the cement. Our interest, in this case, relates to the von Mises stress in a spherical frame of coordinate (r, θ, φ), (Fig. 11).

In this part, we proposed five microcavity defects in different positions on the cement cut plane analyzed by the Ansys workbench code.

In order to demonstrate the effect of the presence of micro-cavities in orthopedic cement on the stress distribution, five different positions of 1mm diameter spherical cavities were tested (Fig. 11). These cavities were oriented at different angles θ = {30°, 60°, 90°, 120°, and 160°} with respect to an axis OZ in a vertical plane contained in a zone under stress.

The effect of the previously discussed implant angle φ posture (φ = 0°) was also examined in combination with the different positions of the cavities.

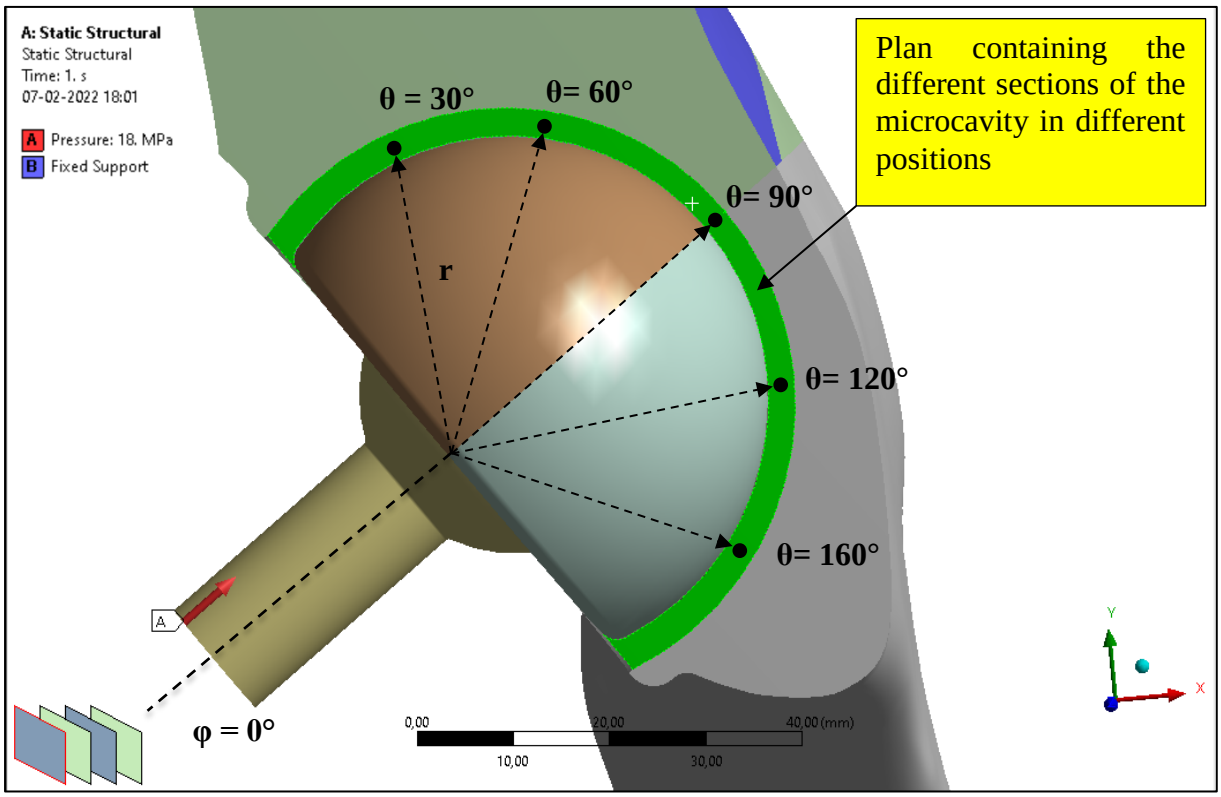

Fig. 11. Position of the microcavity in a spherical frame of reference (r, θ, φ)

Study of convergence of the mesh in the orthopedic cement. Once the meshing method was chosen, the size controls of the mesh were analysed. The main parameters of size control were modified to obtain different meshes with different mesh densities. The mesh density is especially related to the number of nodes and number of elements, and it determines the validity of the results. The results obtained in Table 2 using a mesh with a low number of nodes could be right, but if a mesh with a high number of nodes is used, then the computation time to develop the analysis could be excessively high and the results are not correct. For this reason, a study of convergence of the results should be carried out, in order to ensure that the proper mesh density is chosen and to validate the results. To develop the study of convergence of the results, the analysis of the von Mises stress in the cement was carried out with different mesh densities.

The various analyzes were carried out by increasing the number of nodes, that is to say by increasing the density of nodes in the mesh. The results of Table 2 are transferred to Fig. 12 and Fig. 13 in order to analyze the convergence of the von Mises stress results in the orthopedic cement.

Table. 2. Convergence of von Mises stress results in bone cement for different element sizes

Element Size	Number of elements	Number of nodes	Stress von Mises (MPa)
2 mm	840046	1204720	1.98 MPa
1.75 mm	847494	1217278	2.03 MPa
1.5 mm	867355	1247675	2.04 MPa
1 mm	990809	1432502	2.1 MPa
0.75 mm	1220417	1766613	2.2 MPa
0.5 mm	2163511	3104955	2.78 MPa

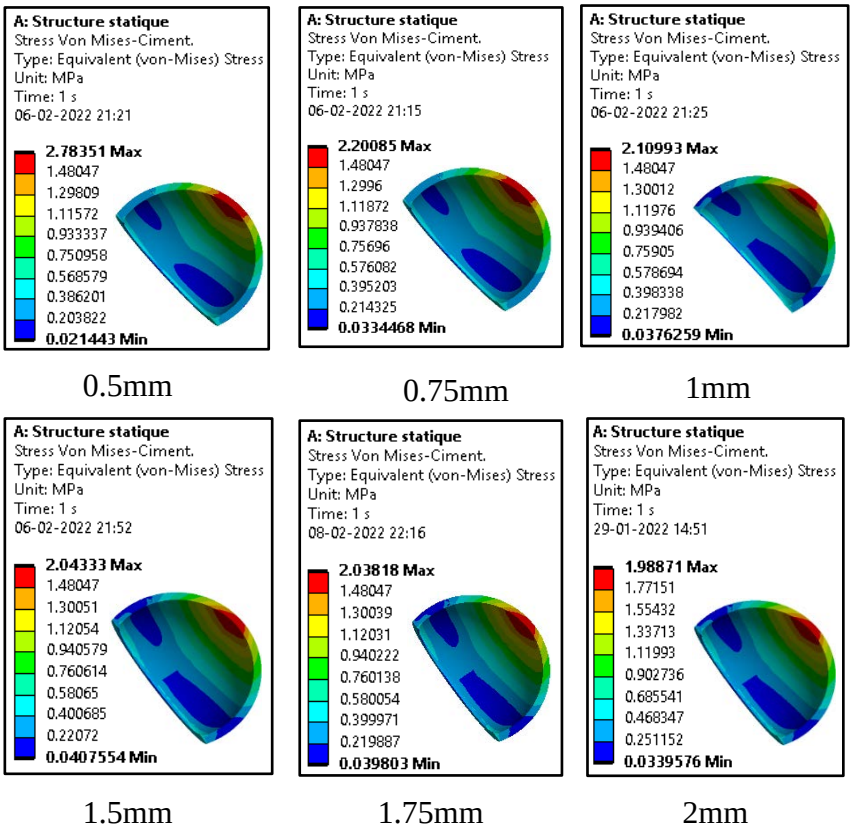

Fig. 12. Convergence of von Mises stress results in orthopedic cement

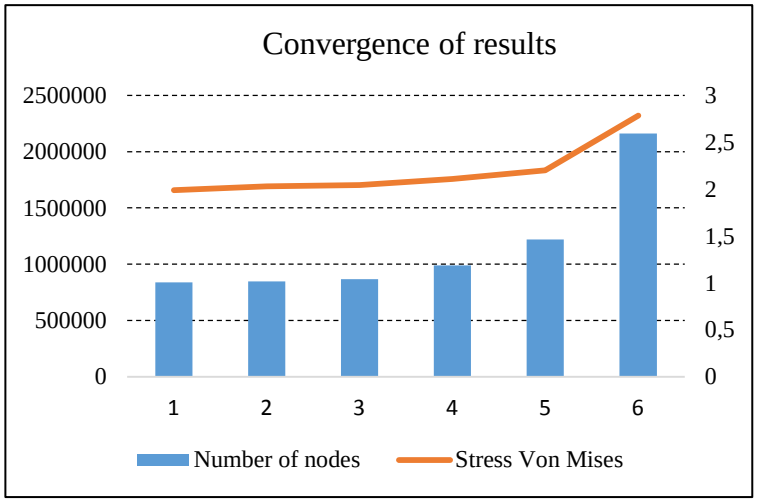

Fig. 13. Convergence of results

We note in Table 2, for the three element sizes (1.5 mm, 1.75 mm, 2 mm), the von Mises stresses in the orthopedic cement are (2.04 MPa, 2.03 MPa, 1.98 MPa) i.e. the von Mises stress convergence stabilizes in all three element sizes (see Fig. 12 and Fig. 13). On the other hand, we notice for a size of elements between 1 mm up to 0.5 mm, the von Mises stresses increase progressively (2.1 Mpa, 2.78 MPa).

It is noted that when an increases the number of nodes, the variation of the results obtained increases. In Fig. 13, we can observe that when the number of nodes is less than 870.000 nodes, a convergence in the results can be observed. On the contrary, when the number of nodes is greater than 870.000, there is a dispersion in the results obtained, i.e. the von Mises stress increases progressively (see Fig. 13).

Figure 14 presents the von Mises stress distribution for different positions of the cavity for an orientation of the implant $\varphi = 0°$. We can notice that for the angles $\theta = 30°$, $\theta = 60°$ and $\theta = 90°$ belonging to the first quadrant, the intensity of the von Mises stresses in the cement increase considerably. For an angle of $\theta = 30°$, the stresses of von Mises equal 1.98MPa, $\theta = 60°$, $\theta = 90°$, the scale of the stresses of von Mises equal to (2.2MPa, 2.97MPa) by the contribution of the other components of THP system.

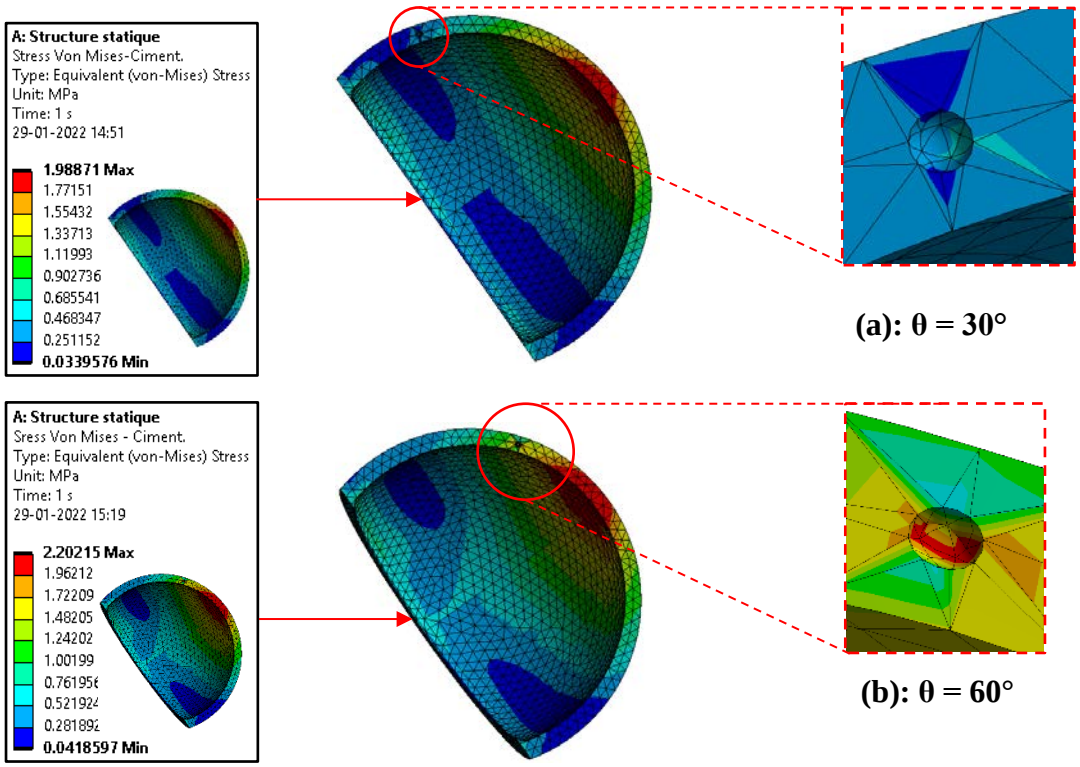

Fig. 14. Different meshes used for different positions of the cavities, (a): $\theta = 30°$, (b): $\theta = 60°$

We can notice that for a microcavity angle $\theta = 120°$ belonging to the first quadrant, the equivalent stresses decrease considerably to a value equal to 2.74MPa (outline in red). Furthermore, for $\theta = 160°$, the stress variations in the cement are very small (1.78MPa) and this is due to their position far from the point of application of the maximum load.

Noting that, all the von Mises stresses obtained for the different positions are tensile stresses varying from $\sigma_{min} = 0.041$MPa to $\sigma_{max} = 2.2$MPa which do not present any danger for the orthopedic cement in comparison with the breaking strength of the latter which is around 25 MPa. The value $\sigma_{max} = 2.2$MPa clearly shows that the presence of micro-cavities within the cement contributes to a significant increase in the stresses in the latter since the maximum stress without cavity was approximately 5.0841MPa (See in Fig. 8).

Figure 14 represents the variations of the von Mises stress in the orthopedic cement for the positions of micro-cavities (θ = 30°, θ = 60°, θ = 90°) depending on the angular position of the implant φ = 0°. The results show that the important values of the von Mises stress in the cavities are equal to (1.98MPa, 2.2MPa, 2.97MPa). Noting that the maximum value is 2.97MPa (in the case where θ = 90°), while the minimum value is 1.78MPa (in the case where θ = 160°).

Figure 15 illustrates the distribution of the von Mises stresses placed along the contour of the cavity at (θ = 30°, θ = 60°, θ = 90°, θ = 120°, θ = 160°) according to the angular position of the implant φ = 0°. Note that the maximum value (σ_{max} = 2.97MPa) is obtained for an inclination angle of the cavity θ = 90°. It should also be noted that the cavity oriented at θ = 120° is subjected in the position of the implant φ = 0° to von Mises stresses, which are relatively low (2.74MPa). In addition, we can observe that the two positions (θ = 30°, θ = 160°) generate the smallest variation in stress which is equal to (1.98 MPa, 1.78MPa).

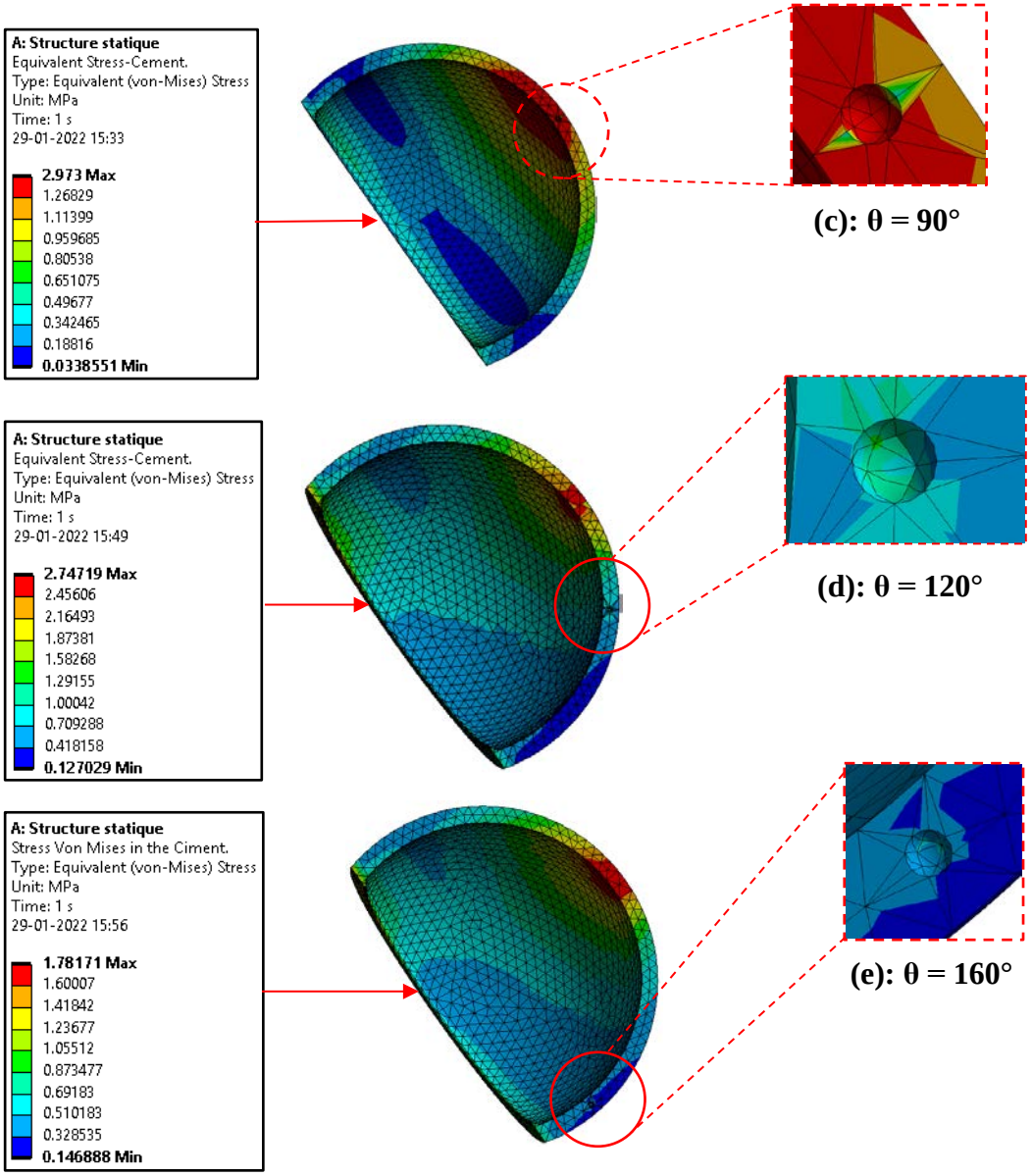

Fig. 15. Different meshes used for different positions of the cavities, (c): θ = 90°, (d): θ = 120°, (e): θ = 160

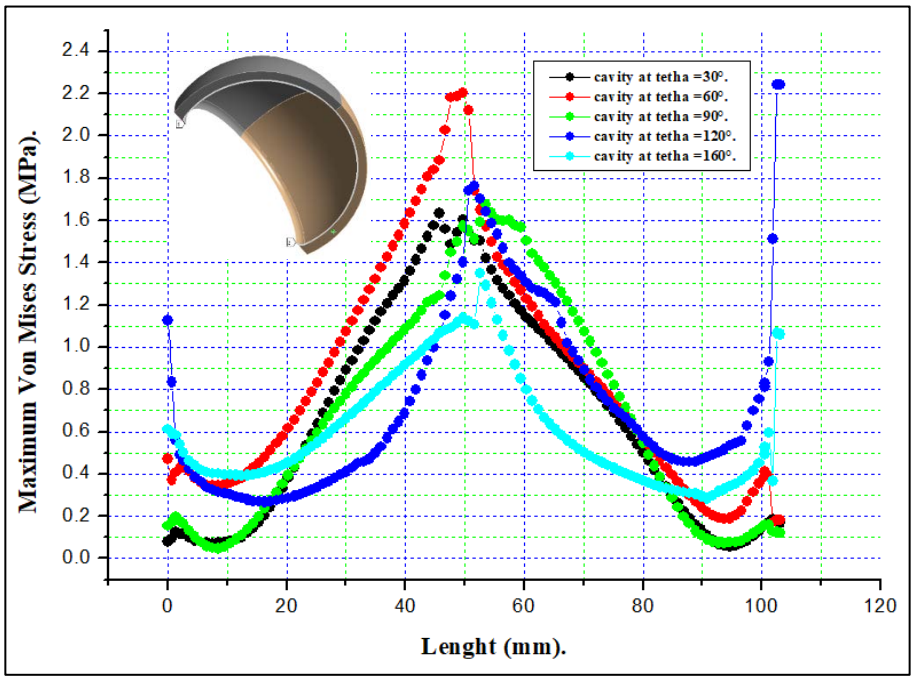

Fig. 16. Comparison of von Mises stresses along the contour for different cavity positions in the case of an implant orientation $\Phi = 0°$

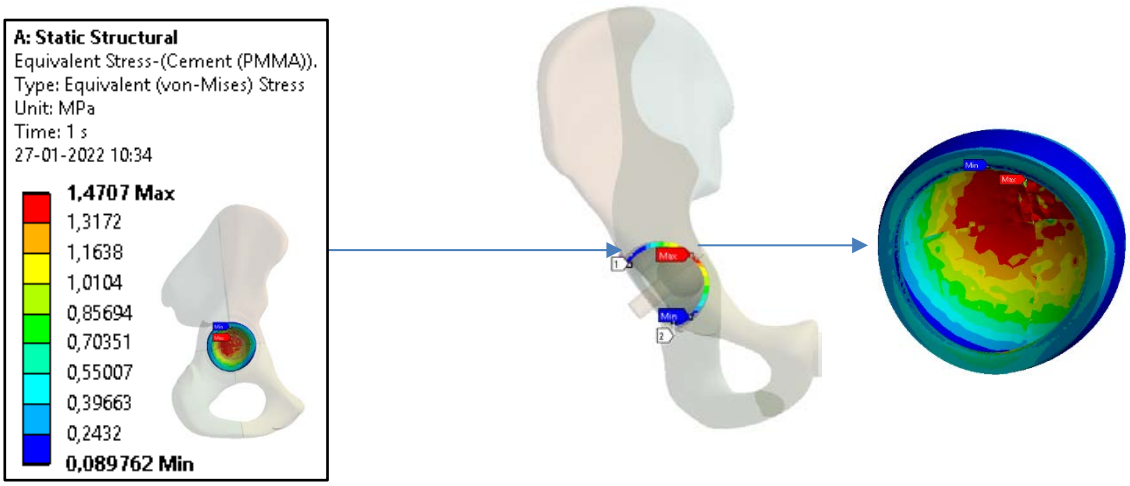

Fig. 17. Distribution of the equivalent stress in the cement, $\varphi = 0°$ and $\theta = 0°$

Noting that, all the stresses obtained for the different positions of the micro-cavities are tensile stresses, which are equal to (1.98MPa, 2.2MPa, 2.97MPa, 2.74MPa, 1.78MPa) which do not present any danger for the orthopedic cement in comparison with the breaking strength of the latter, which is of the order of 25 MPa. The value $\sigma_{max} = 2.97$MPa clearly shows that the presence of micro-cavities within the cement contributes to a significant increase in the stresses in the latter given that the maximum stress without cavity was around 1.47MPa this mentioned in Fig. 16 and Fig. 17.

Effect of semi-elliptical cracks

Effect of the position of semi-elliptical cracks on the distribution of stresses. It is considered that semi-elliptical cracks exist in four positions of the cement A, B, C, and D as

illustrated in Fig. 18. An elliptical crack of major 2c = 4mm and minor axis 2a = 1.2mm is assumed to be located on the left hand of the PMMA and perpendicular to x-axis (Fig. 19). The choice of this zone is due to high stress concentration.

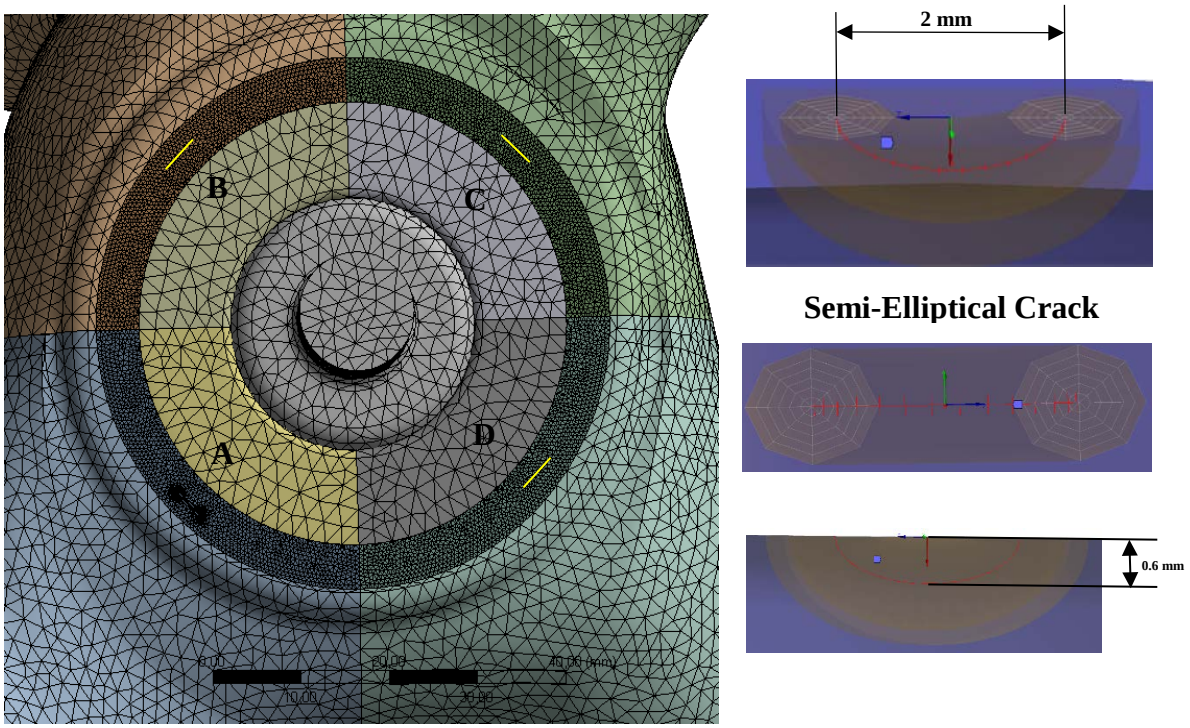

Fig. 18. Model of the mesh and position of semi-elliptical cracks

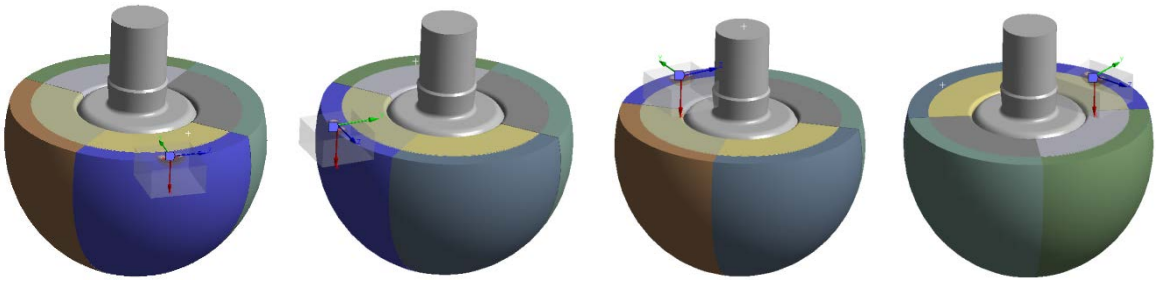

Fig. 19. Location of semi-elliptical cracks in orthopedic cement

Determination of stress intensity factors of orthopedic cement. Finite element analyzes of the cracked reconstruction were performed and stress intensity factor K_b was calculated for each crack point:

$$K_b = \frac{\sigma_{ij}\sqrt{\pi a}}{f_{ij}^{b}(b)}, \tag{1}$$

where b = 1 corresponds to the mode I stress intensity factor (opening mode), b = 2, mode II stress intensity factor (sliding mode), and b = 3, the mode III stress intensity factor (tearing mode).

Toughness is part of the material property in the same way as its elasticity modulus or elastic limit.

$$K_b = \alpha.\sigma_\infty \sqrt{\pi a_c}\ , \tag{2}$$

where a_c is the critical crack length for the stress applied. The objective of this study is to analyze the micro-crack effect on the cement part under high stresses.

Figure 20 presents the stress intensity factors KI (in mode I) along the crack front for four crack positions (A, B, C, and D). It is clear that KI is relatively higher for two crack positions. The crack position B, and C in the x-axis direction has a relatively higher KI compared to positions A and D.

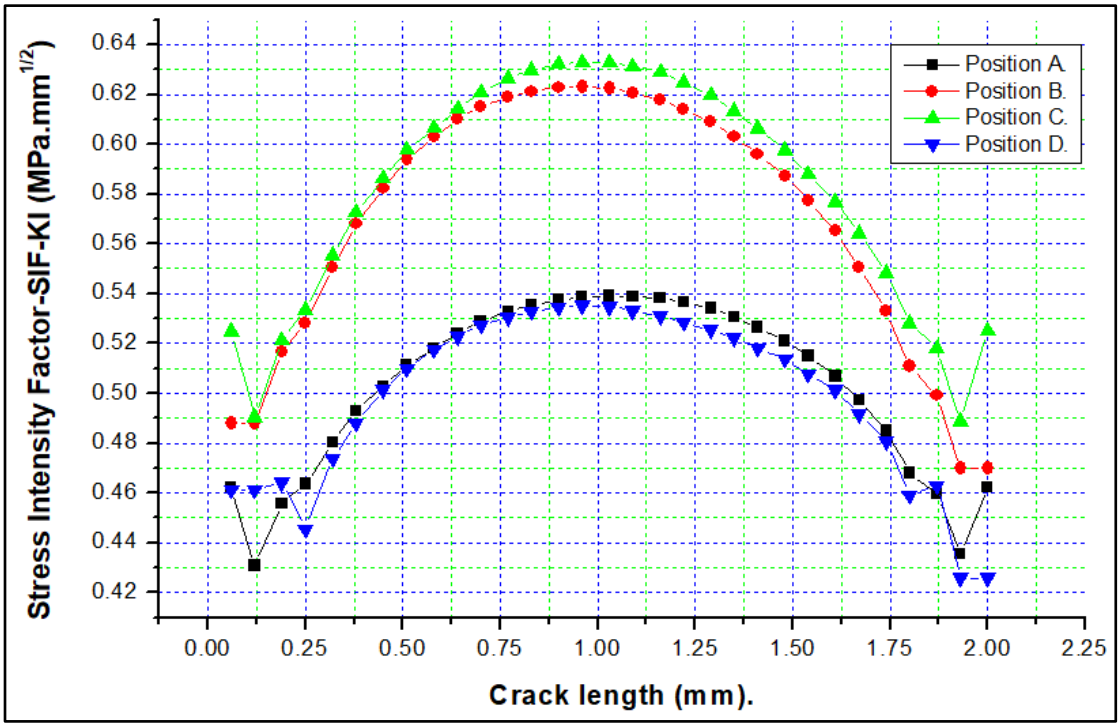

Fig. 20. Distribution of K_I along the crack front for different crack positions

We note in Fig. 20, that a change of semi-elliptical crack position on the orthopedic cement affects the variation of the KI stress intensity factor and J integral. The crack positions (B, C) on the cement orthopedics indicate KI and J maximum which values are equal to (0.62MPa.mm$^{0.5}$, 0.0001836mJ / mm²) and (0.63MPa.mm$^{0.5}$, 0.0001880mJ / mm²) with respect to other positions (A, D) (see Fig. 23 and 24).

It is noted that semi-elliptical crack size (length/depth ratio: c/a = 3.33> 1) considerably affects the distribution of KI and J levels. For crack positions (A, B, C, D), we see in Fig. 20 and 25 that the highest values of KI and J are located in the middle of the crack i.e. crack propagation will initiate from that middle.

Figure 21 shows the stress intensity factor KII (in mode II) along the crack front for four crack positions (A, B, C, D). For a semi-elliptical crack of length 2mm and depth 0.6mm, KII is practically negligible. The crack shear effect is therefore non-existent for these positions.

Figure 22 shows the stress intensity factor KIII (in mode III) along the crack front for four crack positions (A, B, C, D). The KIII value is very low; this is due to the fact that the distribution of the loading is essentially in the xy plane.

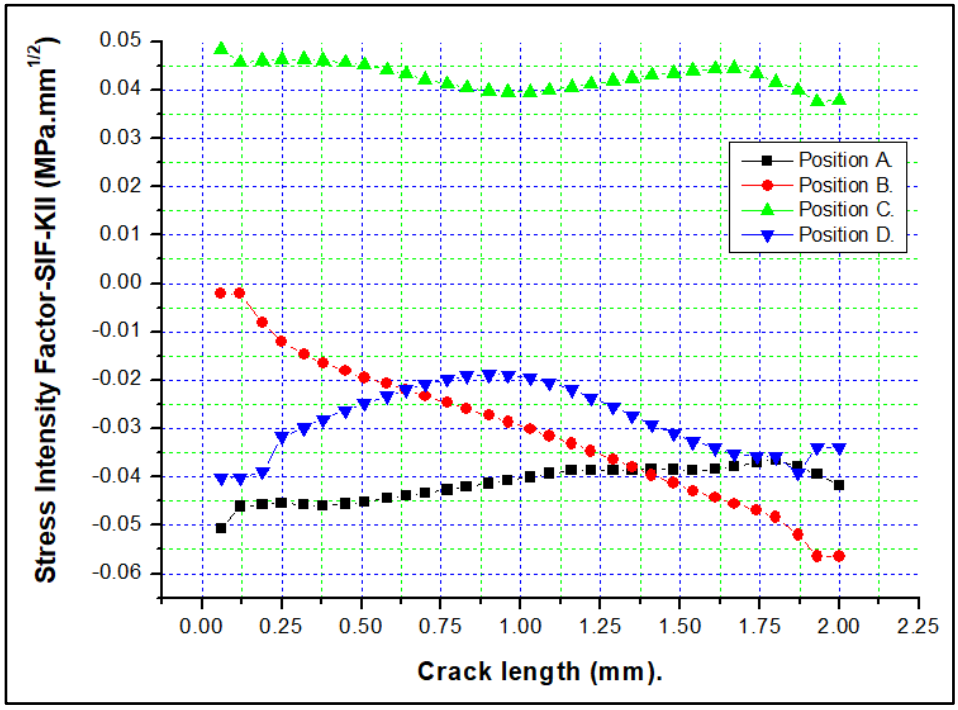

Fig. 21. Distribution of K_{II} along the crack front for different cracks positions

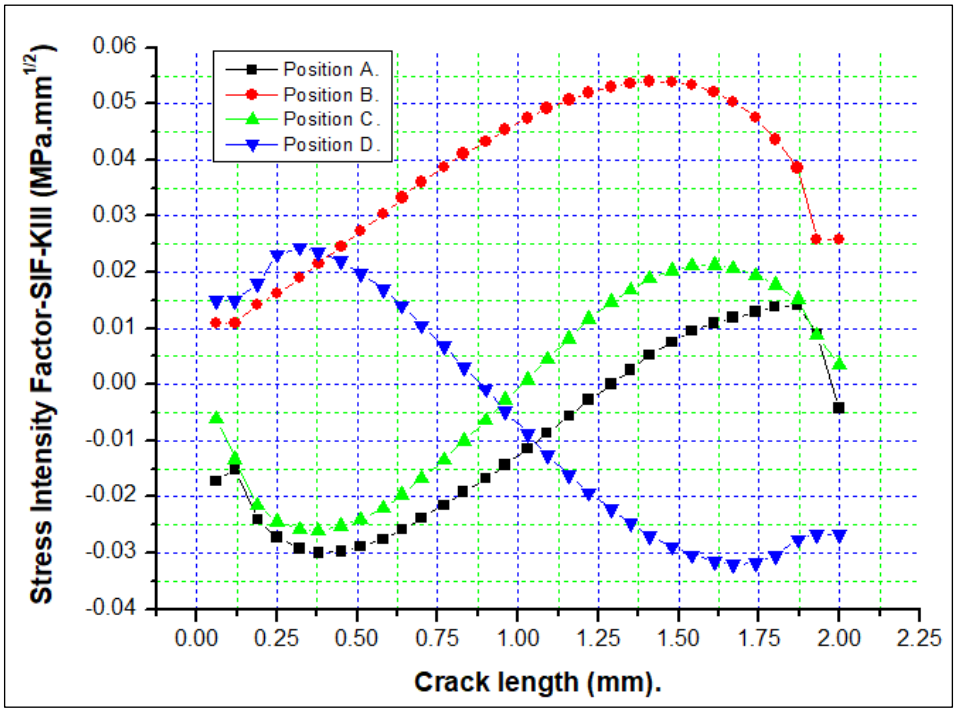

Fig. 22. Distribution of K_{III} along the crack front for different cracks positions

SIF evolution for different cracks positions.

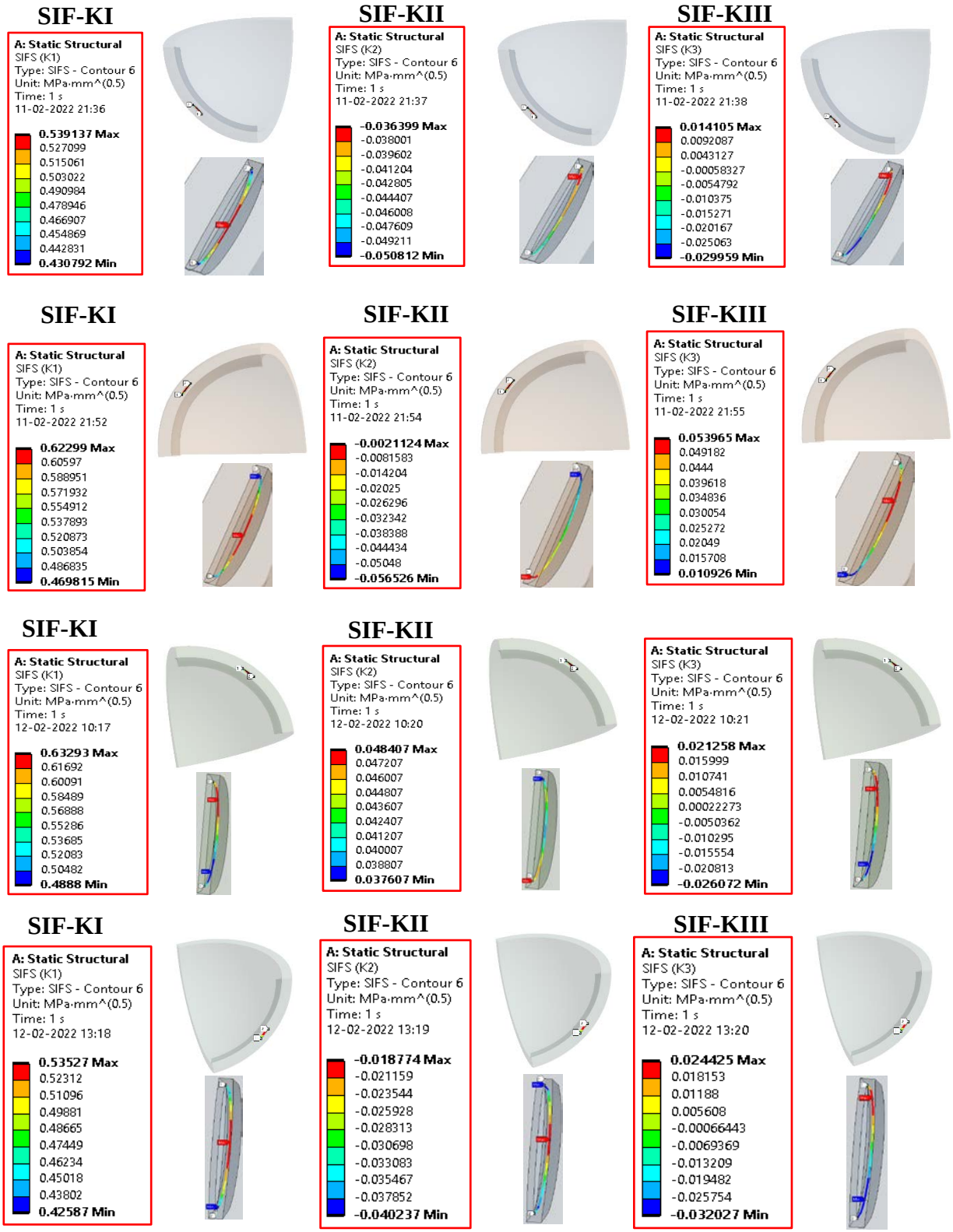

Fig. 23. Distribution of stress intensity factors for different cracks positions

Determinatıon of J-ıntegral (JINT).

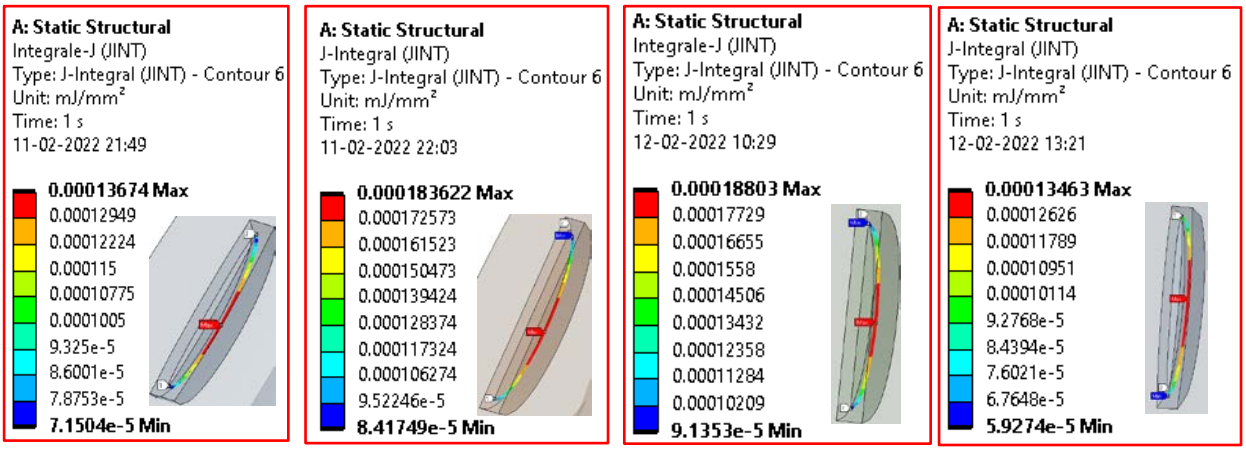

Fig. 24. Distribution of J-integral (JINT) along the crack front for different cracks positions

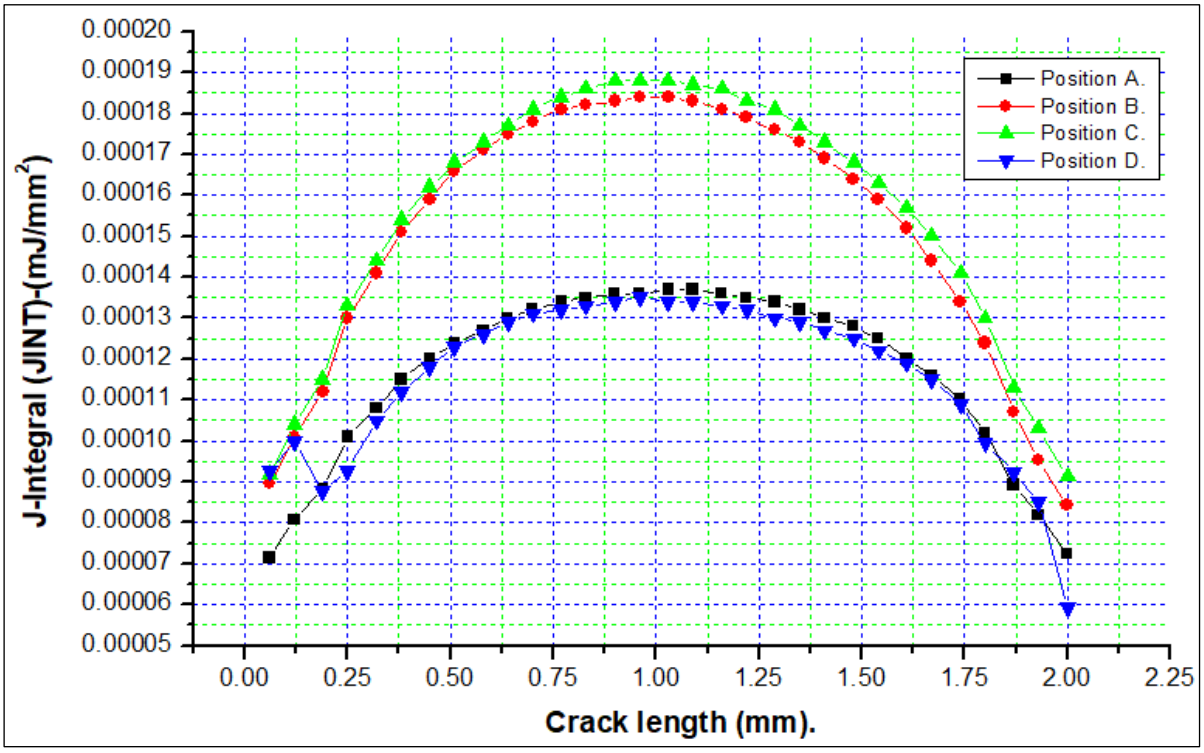

Fig. 25. Distribution of J-integral (JINT) along the crack front for different cracks positions

Figure 26 shows the distribution of von Mises stresses in the coxal-bone, cement, and plastic cup for different positions of the fissures. It can be noticed that the two positions of the semi-elliptical cracks (B, C) indicate maximum stresses at basin levels which are equal to (18.163MPa) respectively are greater than the two positions (A, D).

Figure 26 represents the legend of the von Mises stress in the orthopedic cement for different positions of semi-elliptical cracks. The results show that the important values of the von Mises stress in the cement are obtained for the two positions (B, C), while the lowest values are obtained for the two positions (A, D).In this case, we also noticed that the von Mises stress are symmetric between them.

On the other hand, the two positions of the crack (A, D) show maximum von Mises stresses with respect to the two positions (B, C). Noting that the maximum value is 4.24 MPa, while the minimum value is 3.86 MPa.

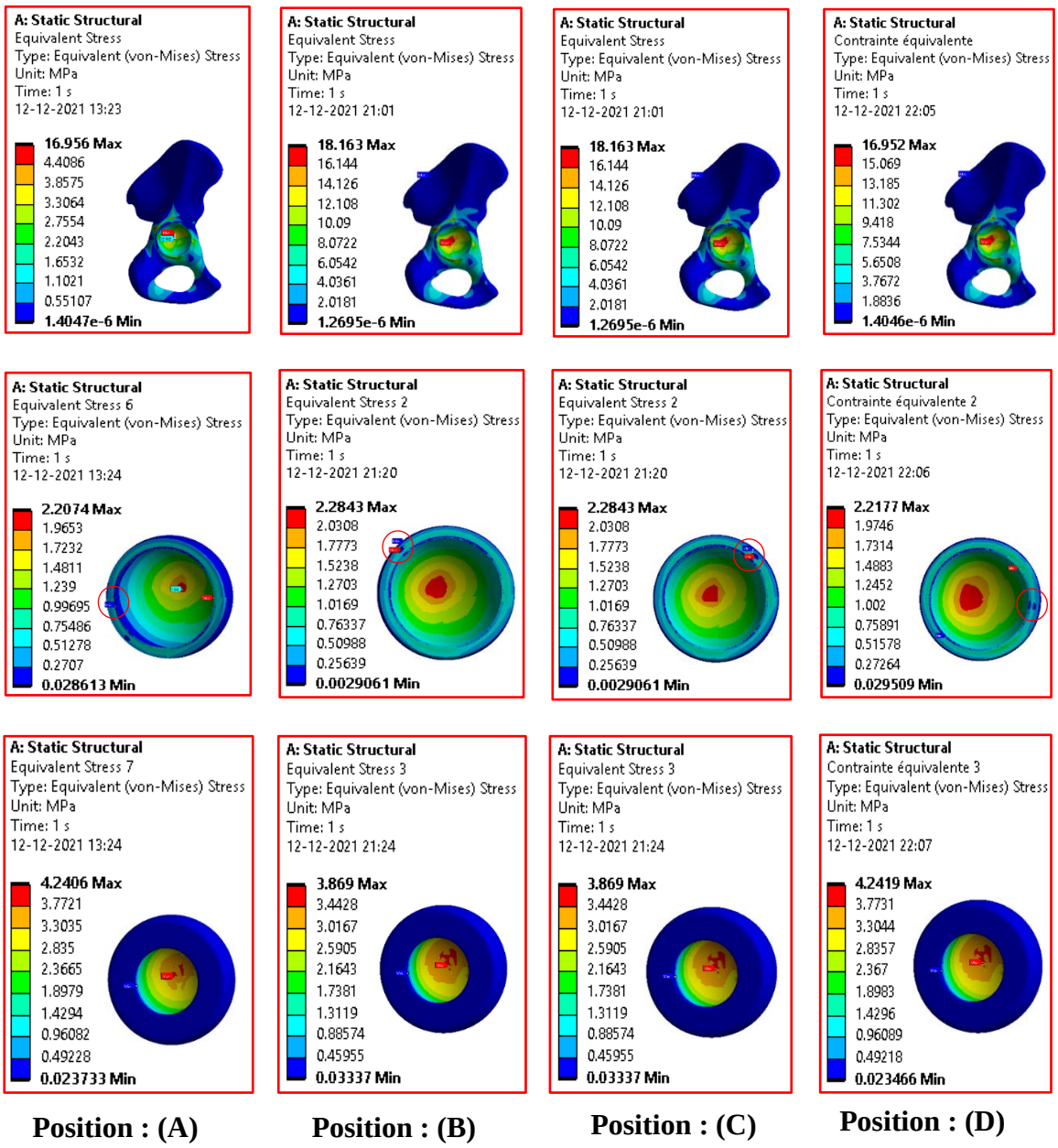

Fig. 26. Distribution of stress intensity factors for different crack positions

5. Conclusion

In orthopedic surgery and more particularly in total hip arthroplasty, the fixing of the implants is generally carried out by means of a surgical cement called (PMMA). This cement must ensure good adhesion between the constituents of the THP on the one hand and others to ensure a good transfer of the load, this element as if fragile, the stress gradient directly influences the functionality of the latter, which promotes the appearance of fractures. The first part of this work studied and analyzed the von Mises stress distribution in orthopedic cement around a spherical microcavity. The second part of this work studied the effect of four positions of the semi-elliptical cracks of length (c=1mm) and depth (a=0.6) located in the

cement of the reconstructed acetabulum by calculating the factors of stress intensity (KI, KII, KIII) and the J-integral along the crack front by the finite element method. We note in this work that the stress values were high when the implant is oriented with respect to the axis of the cup with orientation angles $\alpha = 60°$ and $\alpha = 120°$. For the implant position $\alpha = 0$, the maximum stresses are recorded respectively for the cavities oriented at $\theta = 60°$ and $\theta = 120°$, and the minimum stresses are recorded for $\theta = 30°$, $\theta = 90°$, and $\theta = 160°$ corresponds to the position of the implant $\alpha = 0$. On the other hand, we notice in this study a considerable increase in the von Mises stresses of about 29.73% was observed under the effect of the presence of a cavity in the orthopedic cement. The risk is greater when the microcavity is located in orientation of $\theta = 60°$ and $\theta = 120°$ (high-stress field). For the loading conditions applied, the ends of the cement part are stressed to resist the tensile forces. This can pose a significant risk of crack initiation, as the cement does not resist traction well. It is clear that KI is relatively higher for the two crack positions (B and C) compared to the other positions (A and D). We concluded that the two mechanical defects (microcavity, semi-elliptical crack) show more intense stresses in the THP components and record a very intense level of stress and stress intensity factor KI. These mechanical defects cause damage to the PMMA around the tip of the bone debris, which favors the state of loosening of the total hip prosthesis.

References

[1] Herberts P, Malchau H. Long-term registration has improved the quality of hip replacement A review of the Swedish THR Register comparing 160,000 cases. *Acta Orthopaedica Scandinavica.* 2000;71(2): 111-121.

[2] Foucat D. *Effects of the presence of a metallic grid within the cement for sealing the cupules of total hip prostheses: Mechanical and thermal study. Doctoral thesis*. Strasbourg: Louis Pasteur University; 2003.

[3] Zahaf S, Kebdani S. Biomechanical Study between the Rigid and Dynamic Fixation Systems of the Spinal Column Analyzed by the Finite Element Method. *Nano Biomed. Eng.* 2017;9(2): 169-183.

[4] Charnley J. *Low friction arthroplasty of the hip, Theory and practice*. Berlin: Springer; 1979.

[5] Zahaf S, Mansouri B, Belarbi A, Azari Z. Obesity Effect on the Spine. *Advances in Bioscience and Biotechnology*. 2015;6(8): 556-571.

[6] Bhambrik SK, Gilbertson LN. Micro mechanisms of fatigue crack initiation and propagation in bone cements. *Journal of Biomedical Materials Research*. 1995;29: 233-237.

[7] Danny V, Wehmeyer M, Kebbach M, Heyer H, Bader R. Stress and strain distribution in femoral heads for hip resurfacing arthroplasty with different materials: A finite element analysis. *Journal of the Mechanical Behavior of Biomedical Materials*. 2021;113: 104115.

[8] Lewis G. Properties of acrylic cement. State of the art review. *Journal of Biomedical Materials Research*. 1997; 38(2): 155-182.

[9] Charnley J. Arthroplasty of the hip. A new operation. *The Lancet.* 1961;277(7187): 1129-1132.

[10] Sanjay D, Mondal S, Bhutani R, Ghosh R. The effect of cement mantle thickness on strain energy density distribution and prediction of bone density changes around cemented acetabular component. Proceedings of the Institution of Mechanical Engineers, Part H: *Journal of Engineering in Medicine*. 2018;(232)9: 912-921.

[11] Jamari J, Saputra E, Anwar IB, Van Der Heide E. Study of an additional layer of cement mantle hip joints for reducing cracks. *Journal of Functional Biomaterials.* 2019;10(3): 40.

[12] Kumar A, Ghosh R, Kumar R. Effects of interfacial crack and implant material on mixed-mode stress intensity factor and prediction of interface failure of cemented acetabular

cup. *Journal of Biomedical Materials Research Part B: Applied Biomaterials.* 2020;108(5): 1844-1856.
[13] Abdel-Wahab AA, Silberschmidt VV. Numerical modeling of impact fracture of cortical bone tissue using X-FEM. *Journal of Theoretical and Applied Mechanics*. 2011;49(3): 599-619.
[14] Babić M, Verić O, Božić Ž, Sušić A. Finite element modelling and fatigue life assessment of a cemented total hip prosthesis based on 3D scanning. *Engineering Failure Analysis*. 2020;113: 104536.
[15] Ramos A, Relvas C, Completo A, Simoes JA. The formation of cracks at cement interfaces of different femoral stem designs. *European Orthopaedics and Traumatology*. 2013;4: 205-2156.
[16] Griza S, Azevedo TF, dos Santos SV, Tentardini EK, Strohaecker TR. Metallurgical failure analysis of acetabular metal-backed screws. *Engineering Failure Analysis*. 2013;32: 178-187.
[17] Latham KE, Miller JJ. DNA recovery and analysis from skeletal material in modern forensic contexts. *Forensic sciences research*. 2019;4(1): 51-59.
[18] Najafi AR. Propagation of microcracks in bovine osteonal cortical bone. *Akademeia*. 2011;1: 1923-1504.
[19] Babić M, Verić O, Božić Ž, Sušić A. Fracture analysis of a total hip prosthesis based on reverse engineering. *Engineering Fracture Mechanics*. 2019;215: 261-71.
[20] McCormack BA, Prendergast PJ. Microdamage accumulation in the cement layer of hip replacements under flexural loading. *Journal of Biomechanics*. 1999;32(5): 467-75.
[21] Saputra E, Jamari J, Lie HA, Anwar IB, Ismail R, Tauviqirrahman M, Van Der Heide E. The Effect of Layer Variation Between Liner and Cement Mantle on Reducing Cracks of PMMA Material Hip Joints. *E3S Web of Conferences.* 2018;73: 12013.
[22] De Ruiter L, Cowie RM, Jennings LM, Briscoe A, Janssen D, Verdonschot N. The Effects of Cyclic Loading and Motion on the Implant–Cement Interface and Cement Mantle of PEEK and Cobalt–Chromium Femoral Total Knee Arthroplasty Implants: A Preliminary Study. *Materials.* 2020;13(15): 3323.
[23] Sedmak A, Čolić K, Grbović A, Balać I, Burzić M. Numerical analysis of fatigue crack growth of hip implant. *Engineering Fracture Mechanics.* 2019;216: 106492.
[24] Kocak S, Sekercioglu T. Impact strength of cemented implant interfaces. *Materials Testing*. 2020;62(3): 271-6.
[25] Cherfi M, Abderahmane S, Benbarek S. Fracture behavior modeling of a 3D crack emanated from bony inclusion in the cement PMMA of total hip replacement. *Structural Engineering and Mechanics*. 2018;66(1): 37-43.
[26] Pernod P, Hernigou P. Morphological aspect of cement porosity. *News in Biomaterials.* 1996;3: 235-240.
[27] Zahaf S, Kebdani S. Study and Analysis of Mechanical Behavior between Rigid and Dynamic Fixation Systems Analyzed by the Finite Element Method. *Journal of Biomimetics. Biomaterials and Biomedical Engineering.* 2017;33: 12-31.
[28] Krause W, Mathis RS. Fatigue properties of acrylic bone cement: Review of the literature. *J Biomed. Mater. Res: Applied Biomaterials*. 1988;22: 37-53.
[29] Zahaf S, Mansouri B, Belarbi A, Azari Z. The Effects Induced by a Backpack Eccentric Load on the Spine of Children. *Biomedical Science and Engineering*. 2016;4: 6-22.
[30] Stock J, Verdonschot N, Murphy PB, Predergast PJ, Huikes R. Finite element simulation of anisotropic damage accumulation and creep in acrylic bone cement. *Eng.Fract.Mech.* 2004;71: 513-528.

[31] Zahaf S, Kebdani S, Dahmane M, Azari Z. Biomechanical Comparison between Two Models of the Lumbar Intersomatic Fusion Cage Analyzed by the Finite Element Method. *Journal of Biomimetics, Biomaterials and Biomedical Engineering.* 2017;32: 40-58.
[32] Tong J, Wong KY. Mixed mode fracture of reconstructed acetabulum. In: *Proceeding of the ICF 11 Torino*; 2005.
[33] Bergmann G, Deuretzbacher G, Heller M, Graichen F, Rohlmann A, Strauss J, Duda GN. Hip contact forces and gait patterns from routine activities. *Journal of Biomechanics*. 2001;34: 859-871.
[34] Schuller HM, Dalstra M, Huiskes R, Marti RK. Total hip reconstruction in acetabular dysplasia. A finite element study. *The Journal of Bone and Joint Surgery [Br]*. 1993;75-b: 468-474.
[35] Dalstra M, Huiskes R. Load transfer across the pelvic bone. *Journal of Biomechanics*. 1995;28(6): 715-724.
[36] Nocollela PN, Thacker BH, Katoozian H, Davy DT. Probalistic risk analysis of cemented hip implant. *Bioengineerion Conférence, BED*. 2001;50: 427-428.
[37] Colombi P. Fatigue analysis of cemented hip prosthesis, Model definition and damage evolution algorithm. *Int. Journal of Fatigue*. 2002;24(8): 739-746.
[38] Lennon AB, Pendegast PJ. Evaluation of cement stresses in finite element analysis of cemented orthopaedic implants. *J. Biomech Eng*. 2001;123(6): 623-628.
[39] Harigan TP, Harris WH. A finite element study of the effect of diametral interface gaps on the contact area and pressure in uncemented cylindrical femoral total hip components. *J. Biomech*. 1991;24: 87-91.
[40] Sim E, Freimuller W, Reiter TJ. Finite element analysis of the stress distribution in the proximal end of the femur after stabilization of pertrochantric model fracture: a comparison of two implants. *Injury*. 1999;26(7): 445-9.
[41] Weinas H, HuiskesR, Van ribergen B, Summer DR, Turner TM, Galante JO. Adaptative bone remodelling around bonded noncemented total hip arthroplasty. A comparison between animal experiments and computer simulation. *J. of Orthopaedic Research*. 1993;11: 500-513.
[42] Doblaré M, Garcia JM. Anisotropic bone remodelling model based on damage repair theory to the analysis of the proximal femur before and after total hip replacements. *J. of Biomechanics*. 2001;35(1): 17.
[43] Delaunay C. Charnley total prosthesis: where is the "gold standard" of primary hip arthroplasty today. In: *Orthopedic Mastery.* 1999. p.83.
[44] Fessy MH. Double mobilité-Historique. *Maitrise orthopédique.* 2006;152.
[45] Bousnane T, Benbarek S, Sahli A, Serier B, Bachir Bouiadjra BA. Damage of the bone-cement interface in finite element analyses of cemented orthopaedic implants *Periodica Polytechnica Mechanical Engineering.* 2018;62(2): 173-178.
[46] Beautiful JC. History of the treatment of femoral neck fractures. *Practical Rheumatology*. 2009: 33-36.
[47] Sennou S. A Surgical treatment of femoral neck fractures by percutaneous screwing. *Medical thesis.* 2007;48.
[48 Anderson AE, Peters CL, Tuttle BD, Weiss JA. Subject-specific finite element model of the pelvis: development, validation and sensitivity studies. *Journal of biomechanical engineering.* 2005;127(3): 364-73.
[49] Allaoua F, Habib L, Abderrahmane B. Finite Element analysis of stress state in the cement of total hip prosthesis with elastomeric stress barrier. *Frattura ed Integrità Strutturale*. 2021;15(57): 281-290.
[50] Ouinas D, Flliti A, Sahnoun M, Benbarek S, Taghezout N. Fracture behavior of the cement mantle of reconstructed acetabulum in the presence of a microcrack emanating from a microvoid. *International Journal of Materials Engineering.* 2012;2(6): 90-104.

[51] Azari F, Sas A, Kutzner KP, Klockow A, Scheerlinck T, van Lenthe GH. Cemented short-stem total hip arthroplasty: Characteristics of line-to-line versus undersized cementing techniques using a validated CT-based finite element analysis. *Journal of Orthopaedic Research.* 2021;39(8): 1681-1690.
[52] Rodriguez LC, Chari J, Aghyarian S, Gindri IM, Kosmopoulos V, Rodrigues DC. Preparation and characterization of injectable brushite filled-poly (methyl methacrylate) bone cement. *Materials.* 2014;7(9): 6779-95.
[53] Merckx D. Orthopedic cements in the design of articular prostheses. Biomechanics and biomaterials. SOFCOT teaching notebooks. *French scientific expansion.* 1993;44: 67-76.
[54] Pilliar RM, Vowles R, Williams DF. Note: fracture toughness testing of biomaterials using a mini-short rod specimen design. *Journal of biomedical materials research.* 1987;21(1): 145-54.
[55] Soltész U. The influence of loading conditions on the life-times in fatigue testing of bone cements. *Journal of Materials Science: Materials in Medicine.* 1994;5(9-10): 654-6.
[56] Ries MD, Young E, Al-Marashi L, Goldstein P, Hetherington A, Petrie T, Pruitt L. In vivo behavior of acrylic bone cement in total hip arthroplasty. *Biomaterials.* 2006;27(2): 256-61.
[57] Speirs A, Slomczykowski M, Orr T, Siebenrock K, Nolte L-P. Three-dimensional measurement of cemented femoral stem stability: an in vitro cadaver study. *Clinical Biomechanics.* 2000;15: 248-255.
[58] Bialoblocka-Juszczyk E, Baleani M, Cristofolini L, Viceconti V. Fracture properties of an acrylic bone cement. *Acta of Bioengineering and Biomechanics*. 2008;10: 21.
[59] Ouinas D, Flliti A, Sahnoun M, Benbarek S, Taghezout N. Fracture behavior of the cement mantle of reconstructed acetabulum in the presence of a microcrack emanating from a microvoid. *International Journal of Materials Engineering*. 2012;2(6): 90-104.
[60] Lamvohee JMS, Ingle P, Cheah K, Dowell J, Mootanah R. Total hip replacement: Tensile stress in bone cement is influenced by cement mantle thickness, acetabular size, bone quality, and body mass index. *Journal of Computer Science and Systems Biology*. 2014;7(3): 72-78.
[61] Zheng L, Chen X, Zheng Y, He X, Wu J, Lin Z. Cement augmentation of the proximal femoral nail antirotation for the treatment of two intertrochanteric fractures-a comparative finite element study. *BMC Musculoskeletal Disorders*. 2021;22(1): 1-13.

THE AUTHORS

Zahaf S.
e-mail: samir.zahaf@univ-dbkm.dz
ORCID: 0000-0002-4138-1562

Dahmane M.
e-mail: m.dahmane@ensh.dz
ORCID: 0000-0002-8510-353X

Belaziz A.
e-mail: belaziz2013@gmail.com
ORCID: 0000-0002-4737-753X

Bouri I.
e-mail: bouri-ing@hotmail.fr
ORCID: 0000-0001-6464-8138

Afane N.
e-mail: afanenasreddine@gmail.com
ORCID: 0000-0001-6689-7314